FABRICATION OF LITHIUM SULFUR CATHODES VIA AIR-CONTROLLED ELECTROSPRAY

A Thesis

Presented to the Faculty of the Graduate School

of Cornell University

In Partial Fulfillment of the Requirements for the Degree of

Master of Science

by

Rui Zhang

December 2018

ABSTRACT

Rechargeable Lithium Sulfur batteries are considered as the next generation electrochemical energy storage system, because of their high theoretical capacity and high energy density. However, before it can be commercialized, the Li-S battery system needs to solve several critical problems including the shuttle effect and solubility of higher order polysulfides and volume expansion. In this thesis, we focused on addressing these issues by applying air-controlled electrospray in cathode fabrication. Then, integration with layer-on-layer structure made it possible to achieve a better performance at a high sulfur loading. Further, a current collector free strategy where sulfur/carbon cathode materials are directly deposited on a separator helped to obtain a higher gravimetric and volumetric energy density.

BIOGRAPHICAL SKETCH

Rui Zhang was born in China, on November 10, 1992. His interest in Science was intrigued at a very young age by his engineer father. He was offered a scholarship from National University of Singapore after graduation of high school. After one year of thinking, he decided to study Chemical Engineering for his career. After four years as undergraduate, Rui Zhang moved to United States to pursue his Master of Science degree at Cornell University. At Cornell University, he studied to work as a researcher developing next generation Lithium Sulfur batteries.

ACKNOWLEDGMENTS

I would like to thank my advisor Professor Yong L. Joo for his patient guidance, encouragement and advice through the learning process of my master program. I would also like to thank my committee member Prof. Lynden Archer for his valuable inputs and suggestions.

I would also like to thank to Dr Jin Hong Lee, Mounica Jyothi Divvela, Willy Halim, and the rest of the Joo group members for their kind help and valuable suggestions.

Finally, I would like to express my gratitude to my parents for their through moral and emotional support in my whole life and for the precious chance to study here in Cornell University.

TABLE OF CONTENTS

CHAPTER 1

Introduction

1.1 Overview of Lithium Sulfur Battery

Electrochemistry was one of the oldest concepts that was invented in the late 1700s. It has more history than the gasoline. So, why do combustion engine cars precede electric vehicles technology? There are several answers that we can point out. Price point, electric vehicles are relatively expensive and hard to maintain, technology point. However, after the advancement of technological device, global warming issue, and popularity on EV, billions of dollars were poured into energy storage R&D. A lot of funding dedicated on the advancement of lithium-based battery.

Unfortunately, the development of lithium ion battery is approaching the theoretical limit. Several new concepts are introduced: Liquid metal batteries, lithium sulfur, lithium air, sodium ion, etc to replace a lithium ion commercially lithium ion battery. Lithium sulfur is one of the promising candidates because of its high energy density, about 3-5 times than the conventional lithium ion battery. Low cost and readily available materials are also another incentive[1–3]. However, problem with sulfur based battery is the poor capacity retention due to intermediate reaction dissolution and migration to the anode sides, called shuttle effect, electronically insulating material, and low active material utilization[1,4]. Those factors inhibit lithium sulfur to reach the maximum potential and hinder the commercialization to compete with lithium ion battery.

Many attempts have been made to circumvent the problems. The most popular one is infusing sulfur particles into mesoporous carbon. Carbon is cheap, abundant, and conductive materials. By the addition of carbon, the electron pathway is created among sulfur network, enhancing sulfur

utilization and improve its performance. There are several types of carbon readily available for sulfur battery implementation: micro/mesoporous carbon (Super P and Ketjen black) [5,6], carbon nanotube[7,8], graphene[9], graphene oxide[10–12], carbon fiber[13,14], etc., which have pro and cons among them. Graphene is a 2D flat carbon material, and it has an excellent conductivity to deliver electrons to the active materials, but it is relatively expensive[9,15]. On the other hand, graphene oxide has a good capability to anchor polysulfides from diffusing to anode material; however, it is relatively insulating because of the myriad oxide groups protruding from the carbon planar[10,12].

For more advanced system like high loading sulfur, 3D host materials are needed as a template [16]. Typically: carbon nanofiber, cellulose fibers, or carbon nanotubes were implemented for a high loading sulfur (>10 mg cm-2). In addition, the addition of carbon nanofiber interlayer is essential to further trap the lithium polysulfides and mitigate the shuttling effect[13]. However, this method is unsuitable for production, because of low gravimetric energy density from the addition of interlayer. The problem with 3D carbon materials is the inflexibility for scaling up. For coin cells, it won't cause big problem, however, when implemented into pouch cells or cylindrical cells, the bending instability will not preserve the structure, and the welding will be challenging as well.

To address the safety issue from the electrolyte, several scientists investigated the possibility of using gel polymer electrolyte (GPE) by crosslinking electrolyte solution with the additives[17]. Sold state battery is gaining more popularity in the electric vehicles application because of the need to prevent casualties. The polymer property prevents the ignition in case of thermal runaway

or short circuit. In addition, solid state battery eliminates the need of separator. However, the lithium ion diffusion is also hindered in the polymer solution and results in low capacity.

In our research, we are focusing on the deposition method by our novel method called air-controlled electrospray process[18,19]. By implementing our process, we obtained a different morphology on the electrode surface. Instead of having a flat, continuous surface. Based on our experience, it enhances the electrolyte penetration and improve the wetting. As a result, lithium ion will be easily diffused through the sulfur particles and more reaction sites will be available, consequently improving the capacity performance of the cell itself. More detailed explanation on air-controlled electrospray process will be described below.

1.2 Air Controlled Electrospray process

Unlike conventional electrospray process, the air-controlled electrospray utilizes a convective air flow jet to accelerate the drying and deposition process[18]. The nozzle is comprised of two concentric cylinders. The solution is ejected from the inner cylinder, while the air propels through outer nozzle, which is connected to a high voltage source. Our studies indicate that the impinging dry air of the air-controlled electrospray process tends to form smaller charged droplets and evaporate solvent faster, resulting in dry solute deposited on the current collector[19]. The evaporation is accelerated due to higher surface area exposed to the surrounding dry air.

In this thesis, the lithium sulfur performance utilizing air-controlled electrospray process will be explained in detail. Chapter 2 will encompass the application of air-controlled electrospray in fabrication of facile one-step cathodes. In Chapter 3, we will discuss the implementation of layer-

layer structure using air-controlled electrospray process to achieve good performance at high sulfur loading. In Chapter 4, we utilized air-controlled electrospray to directly deposit the active materials on partially coated graphene separator. Graphene coating will undoubtedly increase the charge transfer resistance because the lithium ion diffusion is inhibited, but with partially coating graphene on separator, we leave some space for the lithium ion to diffuse to the electrode and perform the electrochemical reaction.

References

[1] A. Manthiram, Y. Fu, Y.-S. Su, Challenges and Prospects of Lithium-Sulfur Batteries, Acc. Chem. Res. (2012). doi:10.1021/ar300179v.

[2] A. Manthiram, S.-H. Chung, C. Zu, Lithium-Sulfur Batteries: Progress and Prospects, Adv. Mater. 27 (2015) 1980–2006. doi:10.1002/adma.201405115.

[3] J. Lochala, D. Liu, B. Wu, C. Robinson, J. Xiao, Research Progress toward the Practical Applications of Lithium–Sulfur Batteries, ACS Appl. Mater. Interfaces. 9 (2017) 24407–24421. doi:10.1021/acsami.7b06208.

[4] N. Deng, W. Kang, Y. Liu, J. Ju, D. Wu, L. Li, B.S. Hassan, B. Cheng, A review on separators for lithium sulfur battery: Progress and prospects, J. Power Sources. 331 (2016) 132–155. doi:10.1016/j.jpowsour.2016.09.044.

[5] A. Jozwiuk, H. Sommer, J. Janek, T. Brezesinski, Fair performance comparison of different carbon blacks in lithium-sulfur batteries with practical mass loadings - Simple design competes with complex cathode architecture, J. Power Sources. (2015). doi:10.1016/j.jpowsour.2015.07.070.

[6] J. Zheng, M. Gu, M. J. Wagner, K. Hays, X. Li, P. Zuo, C. Wang, J.-G. Zhang, J. Liu, J. Xiao, Revisit Carbon/Sulfur Composite for Li-S Batteries, 2013. doi:10.1149/2.013310jes.

[7] A. Barinov, L. Gregoratti, P. Dudin, S. La Rosa, M. Kiskinova, Imaging and Spectroscopy of Multiwalled Carbon Nanotubes during Oxidation: Defects and Oxygen Bonding, Adv. Mater. 21 (2009) 1916–1920. doi:10.1002/adma.200803003.

[8] J. Guo, Y. Xu, C. Wang, Sulfur-impregnated disordered carbon nanotubes cathode for lithium-sulfur batteries, Nano Lett. 11 (2011) 4288–4294. doi:10.1021/nl202297p.

[9] T. Wei, G. Luo, Z. Fan, C. Zheng, J. Yan, C. Yao, W. Li, C. Zhang, Preparation of

graphene nanosheet/polymer composites using in situ reduction–extractive dispersion, Carbon N. Y. 47 (2009) 2296–2299. doi:10.1016/j.carbon.2009.04.030.

[10] L. Ji, M. Rao, H. Zheng, L. Zhang, Y. Li, W. Duan, J. Guo, E.J. Cairns, Y. Zhang, Graphene Oxide as a Sulfur Immobilizer in High Performance Lithium/Sulfur Cells, J. Am. Chem. Soc. 133 (2011) 18522–18525. doi:10.1021/ja206955k.

[11] S. Stankovich, D.A. Dikin, R.D. Piner, K.A. Kohlhaas, A. Kleinhammes, Y. Jia, Y. Wu, S.T. Nguyen, R.S. Ruoff, Synthesis of graphene-based nanosheets via chemical reduction of exfoliated graphite oxide, Carbon N. Y. 45 (2007) 1558–1565. doi:10.1016/j.carbon.2007.02.034.

[12] J.-Q. Huang, T.-Z. Zhuang, Q. Zhang, H.-J. Peng, C.-M. Chen, F. Wei, Permselective Graphene Oxide Membrane for Highly Stable and Anti-Self-Discharge Lithium–Sulfur Batteries, ACS Nano. 9 (2015) 3002–3011. doi:10.1021/nn507178a.

[13] J. Wang, Y. Yang, F. Kang, Porous carbon nanofiber paper as an effective interlayer for high-performance lithium-sulfur batteries, Electrochim. Acta. 168 (2015) 271–276. doi:10.1016/j.electacta.2015.04.055.

[14] M. Rao, X. Song, E.J. Cairns, Nano-carbon/sulfur composite cathode materials with carbon nanofiber as electrical conductor for advanced secondary lithium/sulfur cells, J. Power Sources. 205 (2012) 474–478. doi:10.1016/j.jpowsour.2012.01.047.

[15] X. Liang, C. Hart, Q. Pang, A. Garsuch, T. Weiss, L.F. Nazar, A highly efficient polysulfide mediator for lithium-sulfur batteries, Nat. Commun. (2015). doi:10.1038/ncomms6682.

[16] R. Fang, S. Zhao, P. Hou, M. Cheng, S. Wang, H.M. Cheng, C. Liu, F. Li, 3D Interconnected Electrode Materials with Ultrahigh Areal Sulfur Loading for Li-S

Batteries, Adv. Mater. (2016). doi:10.1002/adma.201506014.

[17] M. Liu, D. Zhou, Y.-B. He, Y. Fu, X. Qin, C. Miao, H. Du, B. Li, Q.-H. Yang, Z. Lin, T.S. Zhao, F. Kang, Novel gel polymer electrolyte for high-performance lithium–sulfur batteries, Nano Energy. 22 (2016) 278–289. doi:10.1016/j.nanoen.2016.02.008.

[18] M. Yamashita, J.B. Fenn, Electrospray ion source. Another variation on the free-jet theme, J. Phys. Chem. 88 (1984) 4451–4459. doi:10.1021/j150664a002.

[19] J. Lee, B. Ko, J. Kang, Y. Chung, Y. Kim, W. Halim, J.H. Lee, Y.L. Joo, Facile and scalable fabrication of highly loaded sulfur cathodes and lithium–sulfur pouch cells via air-controlled electrospray, Mater. Today Energy. 6 (2017) 255–263. doi:10.1016/j.mtener.2017.11.003.

CHAPTER 2

Facile and Scalable Fabrication of Sulfur Cathodes via Air-Controlled Electrospray

2.1 Introduction

With excessive use of fossil fuels in the past centuries, new clean and sustainable energy sources are needed more than ever to address the energy and environmental problems. One of the key challenges is effective methods for energy conversion and storage. The lithium-ion battery is one of the current solutions widely used in portable electronic devices and electric vehicles. However, it has nearly reached its limits in recent years. Among prospective substitutes, the lithium sulfur battery system is attractive because of its high theoretical energy density (2600 Wh kg^{-1}) and high theoretical energy capacity (1675 mAh g^{-1}) [1-4]. Also, the active material, sulfur, is abundant, nontoxic, cost effective and environmental-friendly.

However, lithium sulfur batteries suffer from a few challenges that need to be addressed before commercialization. First, the dissolution of some polysulfide species causes loss of active material and results in high capacity fading. The dissolved high order polysulfides shuttle to the anode, react with lithium and migrate back to the cathode to get re-oxidized. Second, the insulating nature of sulfur and polysulfides increase the cell resistance and hinder the utilization of active materials. Also, sulfur experiences an 80% volume expansion when converting to Li_2S, which may disrupt the cathode structure and block reaction sites. Lastly, the use of toxic electrolyte and lithium metal also raise safety concerns in application. [5,6].

Scientists have been working for decades to address these problems. The most popular method is sulfur impregnation in carbon, such as graphene oxide [4–6], graphene sheets [7,8], carbon nanotube [9,10], carbon nanofiber [11–14], or any functionalized carbon materials [15,16]. The various structures of carbon materials enhance the performance by increasing the conductivity and mitigating polysulfide shuttling at the same time. To commercialize Li-S batteries, high sulfur loading is necessary to enable an operating current density of 4 mAh cm^{-2} to match lithium ion batteries. However, at such a high loading, challenges of lithium sulfur batteries are magnified with more severe shuttling effects and lower sulfur utilization that accelerates cathode degradation. For example, Fang and co-workers proposed a 3D interconnected electrode material[17]. Later, Peng used a Janus separator to gain a high areal capacity at 5.4 mg cm^{-2}[18]. Building a porous and stable nanostructure is one way to provide more efficient conductive pathways and a stronger polysulfide trapping ability at high loading. This can be accomplished by applying the electrospray technique, which also makes it possible for fabrication of facile and scalable electrodes.

Herein, we propose a facile strategy to fabricate a uniformly coated electrode with hybrid microporous structures. Application of the air-controlled electrospray technique makes it possible to control the morphology of cathode by changing spray parameters and obtain a uniform coating with high sulfur loading. The well-developed structure can trap polysulfides and retard the shuttling effect. Also, higher sulfur utilization can be achieved through improved electron transfer from low polarization and fast redox reaction kinetics.

2.2 Experimental Methods

2.2.1 Preparation of Sulfur-Carbon solution

0.8 g of active sulfur material was mixed and grinded with 0.2 g of Ketjen Black. Then, the mixture was heat treated under air at 155^{o}C for 12 hours to ensure sulfur encapsulation in Ketjen Black. The KB/S mixture, graphene and polyacrylic acid were dispersed at 7:2:1 mass ratio in water and IPA at 7:3 volume ratio to have 6% solid content. The solution was sonicated below room temperature for one hour.

2.2.2 Fabrication of sprayed sulfur cathodes

Lithium sulfur cathode solutions were sprayed onto carbon coated aluminum foil using a coaxial needle (12-gauge inside, 16-gauge outside). The infusion rate and distance were kept at 0.05 ml min^{-1} and 10 cm, respectively. The voltage and air pressure were changed to have electrodes sprayed at no electric field (0 kV/ 25 psi), no air (25 kV/ 0 psi) and both electric field and air (25 kV/ 25 psi). The spraying behavior is visualized using a high-speed camera (RedLake MotionPro HS-3 with Nikon MICRO NIKORR 60mm 1:2:8 lens). The images are taken at 1000 frames per second.

2.2.3 Electrolyte Composition

The electrolyte was 1 M of bis(trifluoromethane)sulfonimide lithium salt (LiTFSI) and 0.15 M of lithium nitrate ($LiNO_3$) in a 1:1 volume ratio of 1,2-dimethoxyethane (DME) and 1,3-Dioxolane (DOL). All were purchased from Sigma Aldrich.

2.2.4 Characterization Methods

Thermogravimetric analysis (TGA) was measured with a heating rate of 10 ^{o}C min^{-1} under nitrogen on a TA Instruments Q500. Scanning electron microscopy (SEM) and Energy Dispersive X-ray

(EDX) images were taken on a Tescan Mira3 FESEM.

Electrochemical performances were measured with cathodes in 2032-type coin cells assmbled in an argon-filled glovebox. Cyclic voltammetry and electrochemical impedance spectroscopy (EIS) tests were performed using a potentiostat (BioLogic BCS 815). Cycling and rate capability test were carried out with a battery cycler (MTI Corporation) at room temperature.

2.3 Results and discussion

2.3.1 Air-controlled Electrospray

The spraying process of carbon/sulfur solution, and the effect of air flow and voltage is studied. The radius of the droplets and the size distribution is observed for three cases: i) Electrospray ii) Air spray and iii) Air controlled (AC) electrospray.

In electrospray, 5 different voltage differences are applied without air. Different electric field strength gives different extension and axisymmetric instability on the jet. The coulombic interactions between the surface charges on the jet increase the instability and lead to the jet break-up [19]. With highly conducting Ketjen Black/graphene, an increase in the electric field results in increasing instability growth rate. As a result, smaller size and larger number of droplets are formed at higher voltage. From Figure 2.1, it can be observed that the jet breaking up occurs at the Taylor cone. As the voltage is increased, the size of droplets decreases.

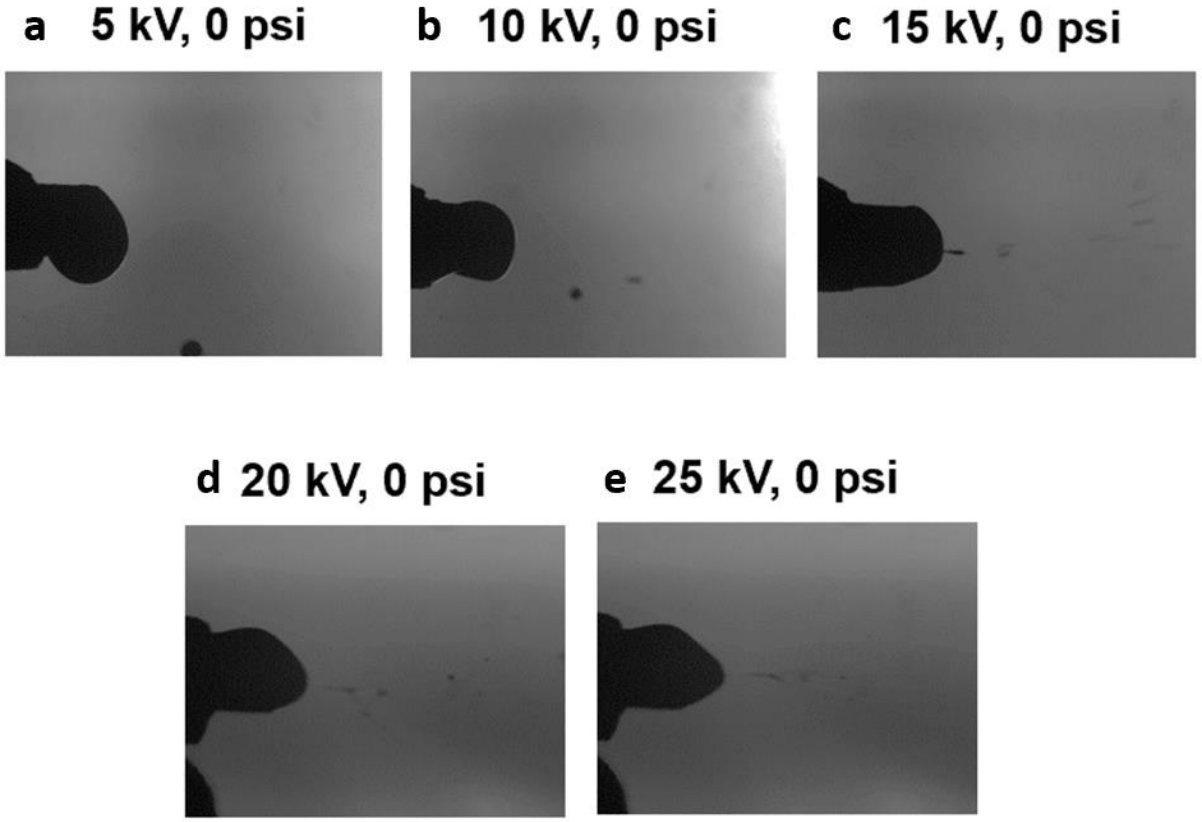

Fig. 2.1. Air spray at voltage a) 5 kV b) 10 kV c) 15 kV d) 20 kV e) 25 kV

In air spray, four different air pressure were applied without any electric field. Jet extension and instability were provided by drag from the air. From Figure 2.2, it can be observed that increasing air pressure decreased the size of the droplets and increased droplet numbers due to the thinner jets formed at high air flow rates. Compared to the electrospray process shown previously, spraying with only air made the process more chaotic and rapid.

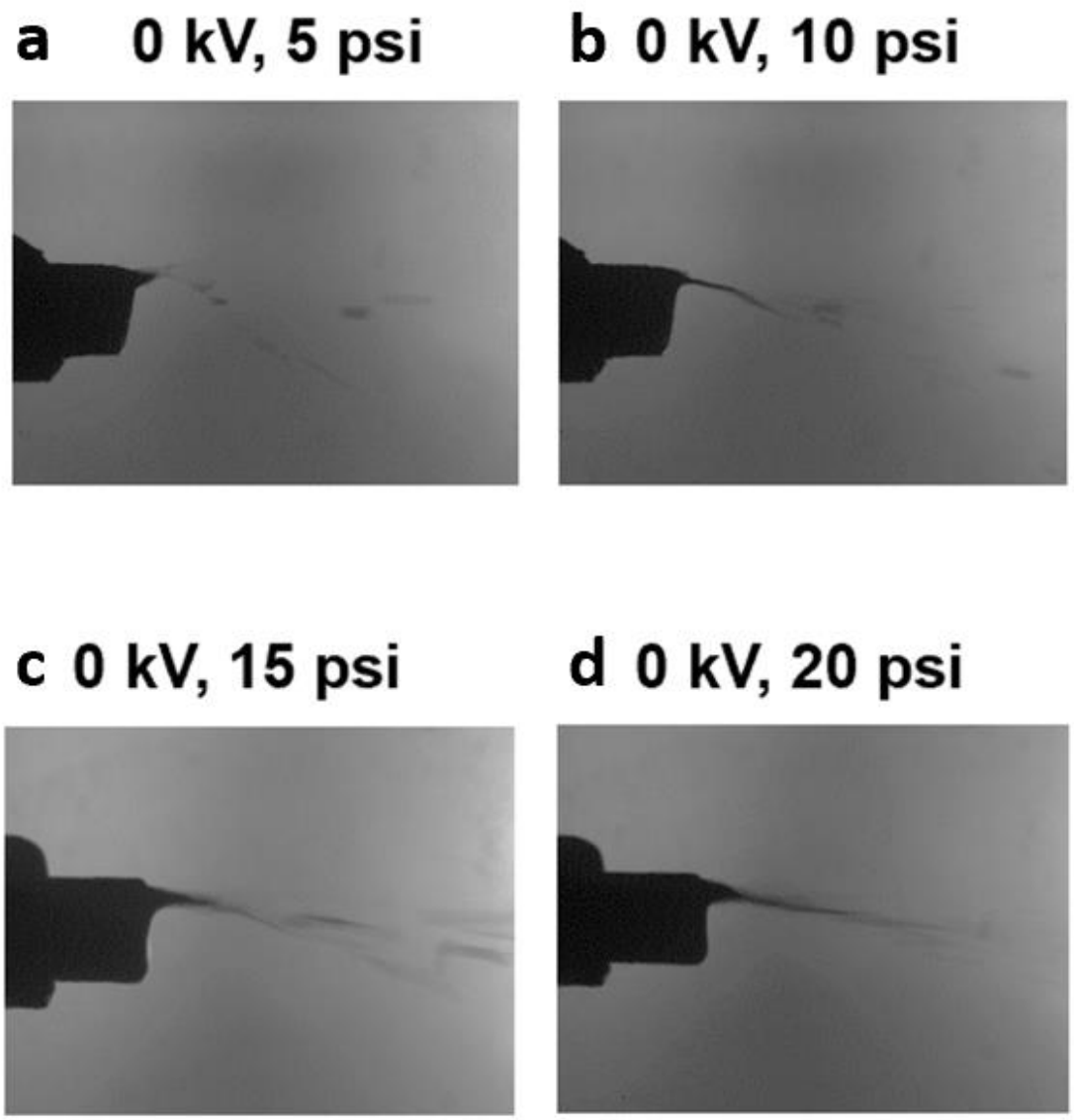

Fig. 2.2. Electrospray at air pressure a) 5 psi b) 10 psi c) 15 psi d) 20 psi

Air-controlled electrospray is a combination of air spray and electrospray as shown in Figure 2.3. Both air pressure and electric field play an important role in the formation of jets and size distribution of droplets. Compared to air spray, the droplet size was more uniform because of the addition of an electric field. As expected, droplet number still increased with increasing air pressure.

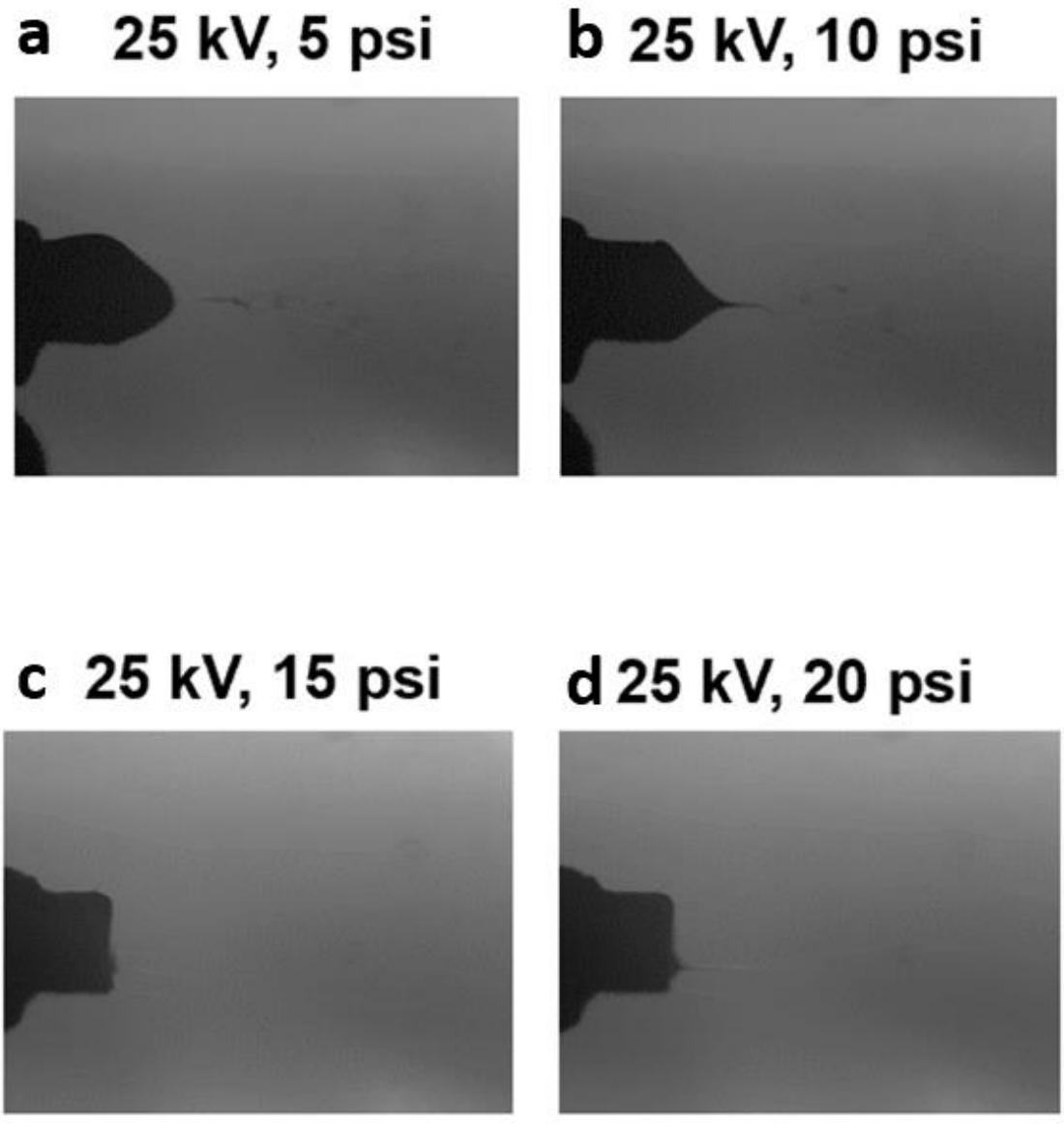

Fig. 2.3. Air-controlled electrospray at voltage 25kV and air pressure

a) 5 psi b) 10 psi c) 15 psi d) 20 psi

Figure 2.4 presents the SEM images for slurry coating, air spray, electrospray and air-controlled electrospray. For slurry coated electrode (Fig 2.4a), the surface image shows a dense layer with cracking, which is the result of the drying process. This will get worse with increasing sulfur loading and electrode thickness [20]. In the spray technique (Fig 2.4 b-d), the morphology highly depends on the parameters, like flow rate, distance, electric field and convective air-flow. In Figure 2.4b, the electrosprayed surface shows a dense surface consisting of inconsistent dark and light color regions. As explained in the previous section, solvent evaporation was not quick enough, and droplet sizes were too big due to lack of instability. With the help of strong air, air spray electrodes showed more uniform coating as shown in Figure 2.4c. Further combining both, a more porous surface was obtained by air-controlled electrospray. The voids and rough surfaces are beneficial as they can accommodate the sulfur expansion and good electrolyte penetration[21].

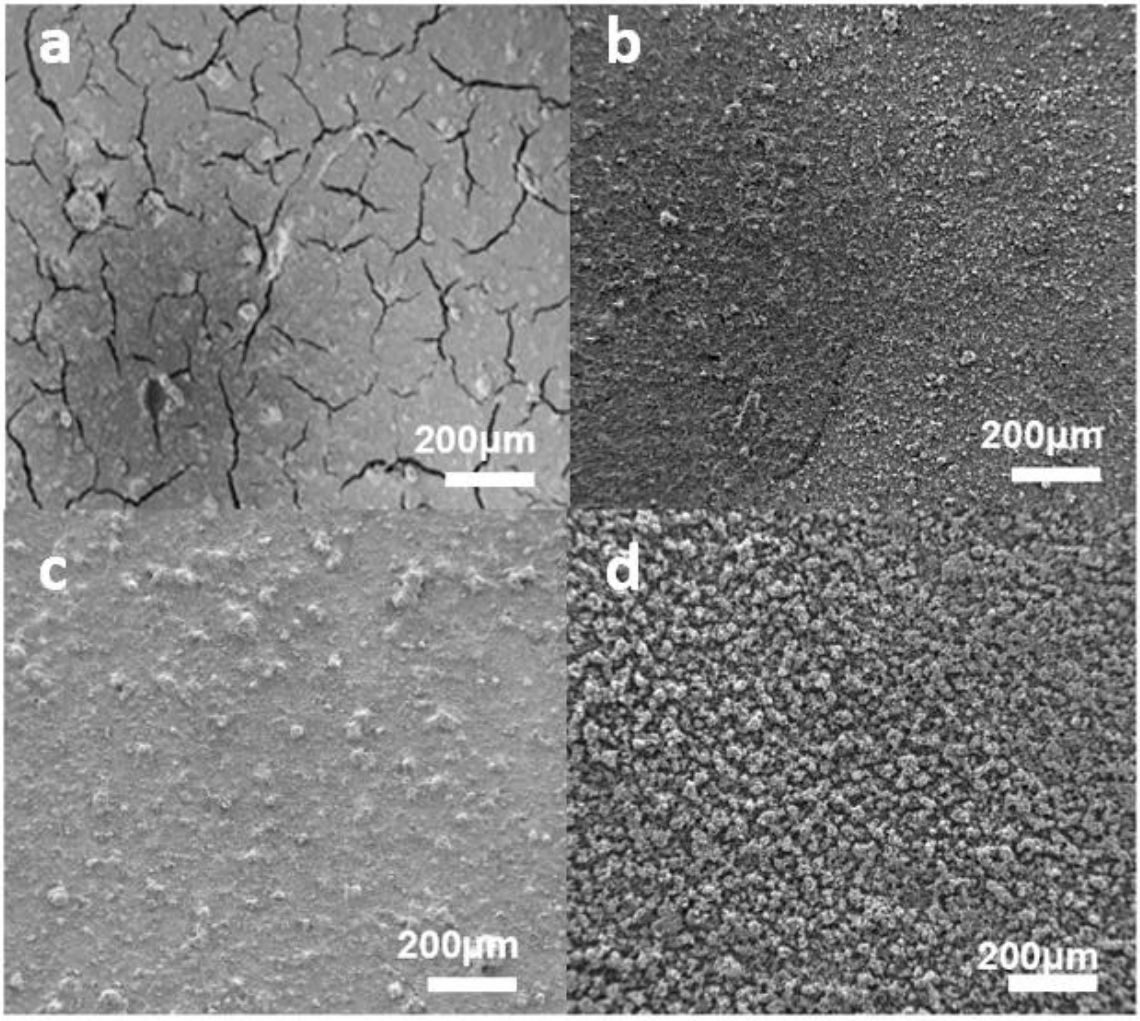

Fig. 2.4. SEM images of cathodes via a) slurry coating, b) electrospray, c) air spray and d) air-controlled electrospray

2.3.2 Electrochemical Performance

To check the consistency of sulfur content after spraying, the active materials were scraped from the aluminum collector for thermogravimetric analysis (TGA). As shown in the Figure 2.5, at 400°C, there was around 35.8% residual, which should consist of Ketjen Black and graphene. If

all 10% of PAA was assumed to be removed, sulfur content can be decided to be 54.2%. This was very closed to the original composition in the solution (56%). The difference could be results from fast evaporation of the convective dry air in the spray process, since not all the sulfur is encapsulated and protected in the pores of Ketjen Black.

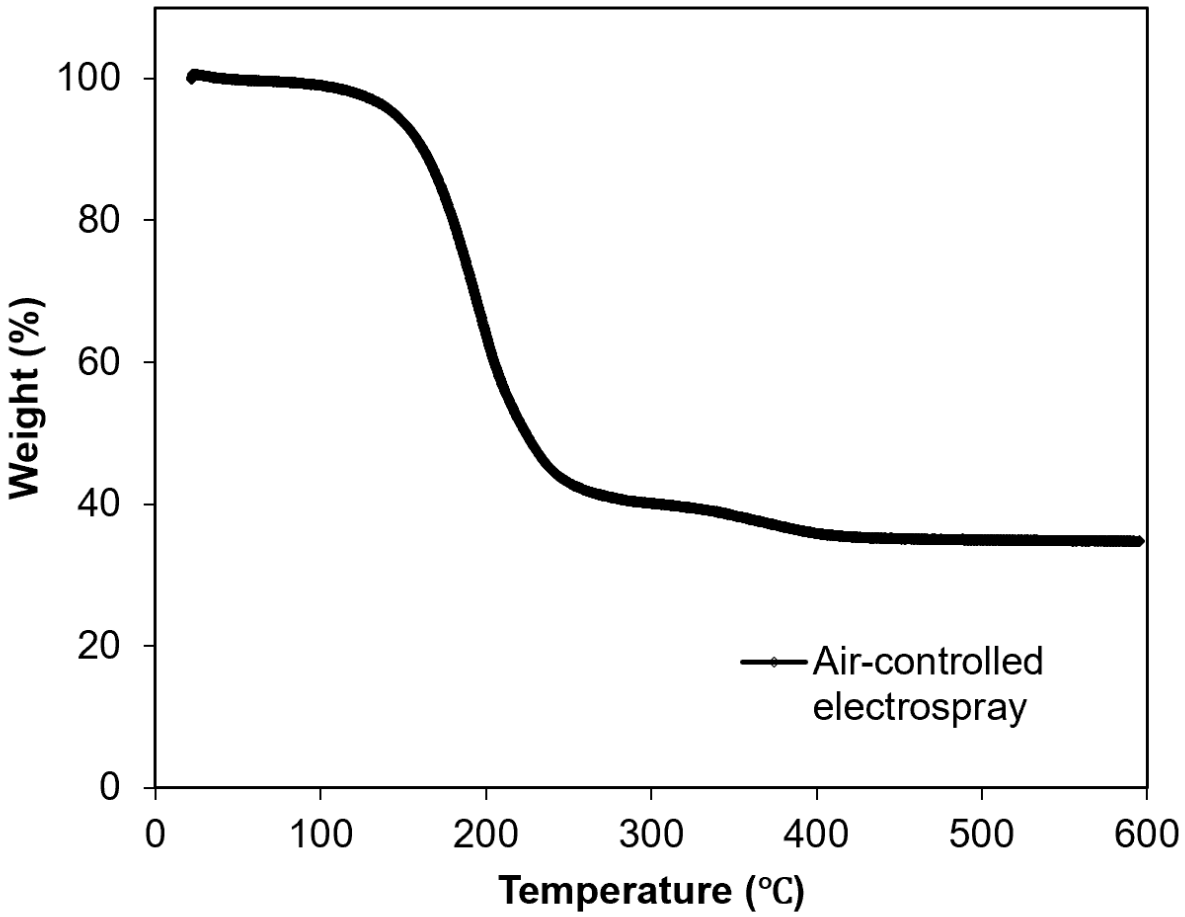

Fig. 2.5. TGA for air-controlled electrospray cathodes

Electrochemical impedance spectroscopy (EIS) results for slurry coating and air-controlled electrospray are shown in (Figure 2.6b). The Nyquist plot in EIS is composed of two parts. At the medium to high frequency region, a depressed semicircle indicates the bulk resistance of electrolyte and charge transfer resistance. At the low frequency region, an oblique line is related

to the diffusion of lithium ions. [22] The sprayed system showed a smaller semicircle width compared to slurry coating electrodes, which corresponds to lower charge transfer resistance. This is due to excellent contact between active materials and carbon materials.

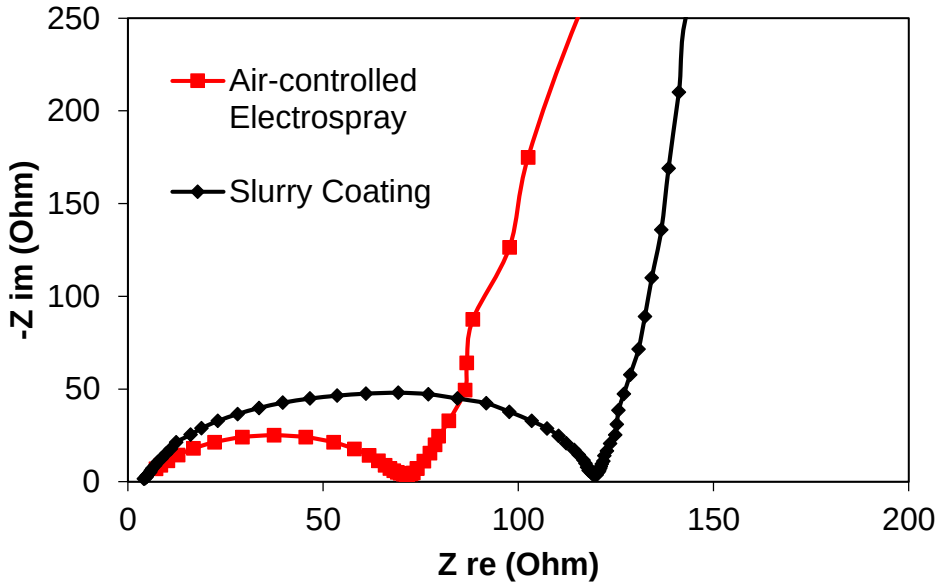

Fig. 2.6. EIS characterization on slurry coating and air-controlled electrospray cathodes

The redox behavior of the slurry coating and air-controlled electrosprayed sulfur cathodes was measured by cyclic voltammetry (CV) at a scan rate of 0.1 mV s^{-1}. As shown in Figure 2.7, the cell with the slurry coated electrode exhibited two broad cathodic peaks and an anodic peak due to the sluggish kinetic process[23]. In comparison, the air-controlled electrosprayed electrode demonstrated an increase in current density, suggesting improved redox reaction kinetics and utilization of the active materials[23-24].

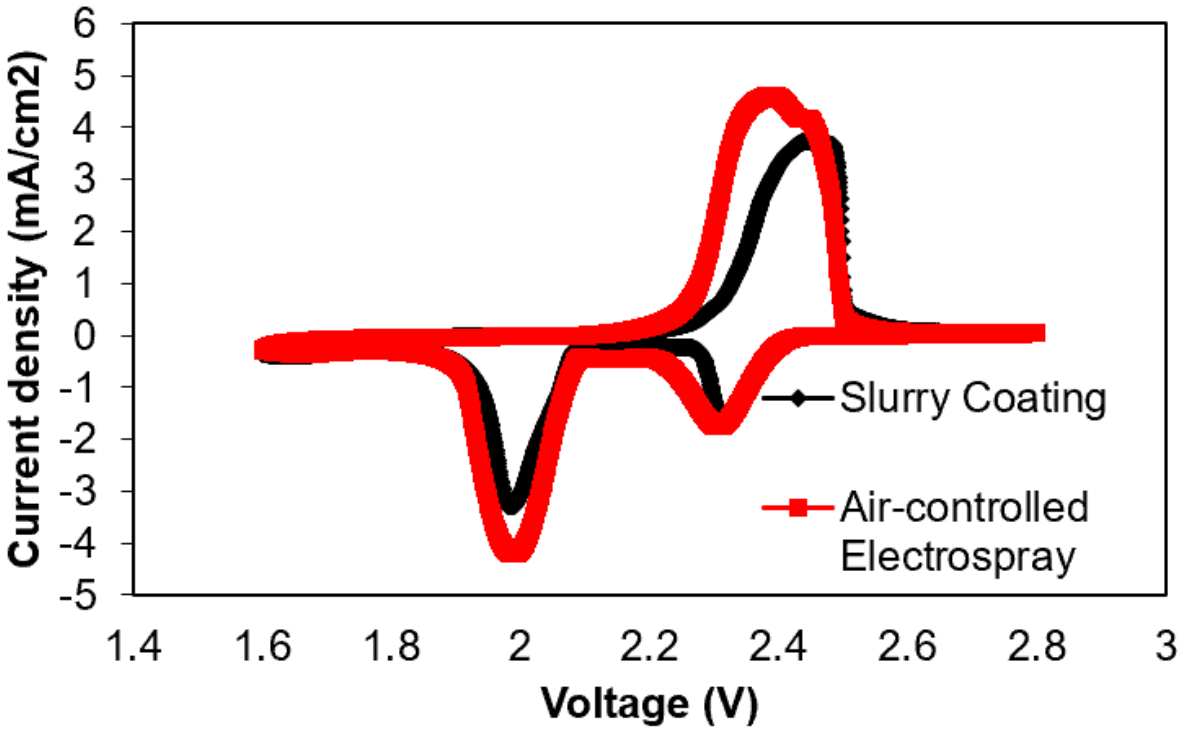

Fig. 2.7. Cyclic voltammogram profiles on slurry coating and air-controlled electrosprayed cathode

Results of cyclability tests conducted at a 0.2 C rate are shown in Figure 2.8. The sulfur loading was kept near 1 mg cm^{-2} for all different system. After an activation of 2 cycles, the discharge capacities of 598.9 mAh g^{-1}, 347.2 mAh g^{-1}, 478.3 mAh g^{-1} and 852.5 mAh g^{-1} were obtained for slurry coating, electrospray, air spray and air-controlled electrospray, respectively. The air-controlled electrospray cell exhibited the highest discharge capacities compared to the reference slurry coating cathode. After 100 cycles, it was more obvious that the air-controlled electrospray cell maintained much more stable cycling with reversible capacity of 742.1 mAh g^{-1}, while the slurry coating cell showed the worst retention among all. The difference came from the cracked surface in slurry coating, which allowed continuous dissolution of lithium polysulfides into the

electrolyte and active material loss. When the sulfur loading was increased to 3 mg cm^{-2}, air-controlled electrospray was still able to present an initial discharge capacity of 839.8 mAh g^{-1}, and a reversible capacity of 538.6 mAh g^{-1} at the 100th cycle. However, electrospray and air-spray didn't produce satisfactory discharge capacities, due to the highly dense surface resulting in smaller surface area available for reaction and poor accessibility of electrolyte. Voltage profile for slurry coating and air-controlled electrospray at their 5^{th} cycle was shown in Figure.2.9 to explore their behavior difference during charge and discharge. It is obvious that there was less overpotential in the air-controlled electrospray cell, this came from the higher conductivity in the system that enabled better kinetics.

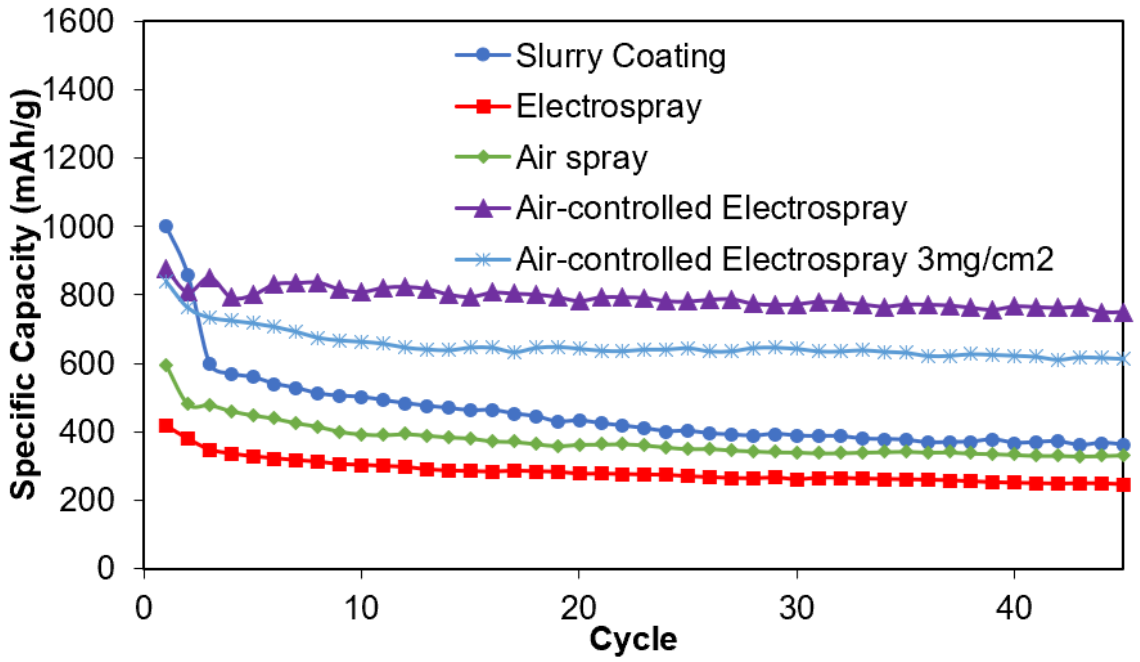

Fig. 2.8. Cycling performance for cells fabricated by slurry coating, electrospray, air spray and air-controlled electrospray

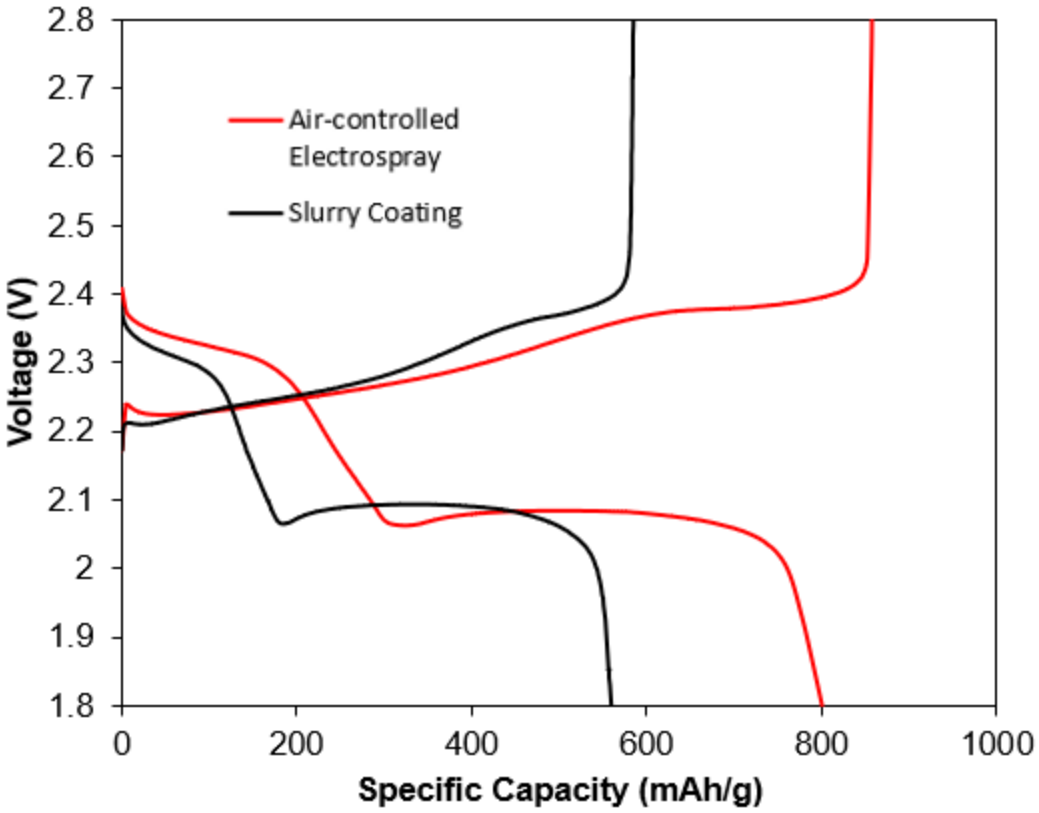

Fig. 2.9. Voltage profile of slurry coating and air-controlled electrospray

The rate capability of cells at different C-rates is presented in Figure 2.10. As expected, the results followed a similar trend as cyclability. The difference in discharge capacities between the sprayed and slurry coating cells was even more conspicuous at high current densities, because of the significance of redox reaction kinetics. At a C-rate of 2 C, the air-controlled electrosprayed cell still maintained 49.9 % of its initial capacity, while the reference slurry coating cathode only had a retention of 7.2 %. A reversible discharge capacity of 756.8 mAh g^{-1} was able to recover after returning to 0.1 C for air-controlled electrospray. At a higher loading of nearly 3 mg cm^{-2}, 32.3% of initial capacity remained at 2C.

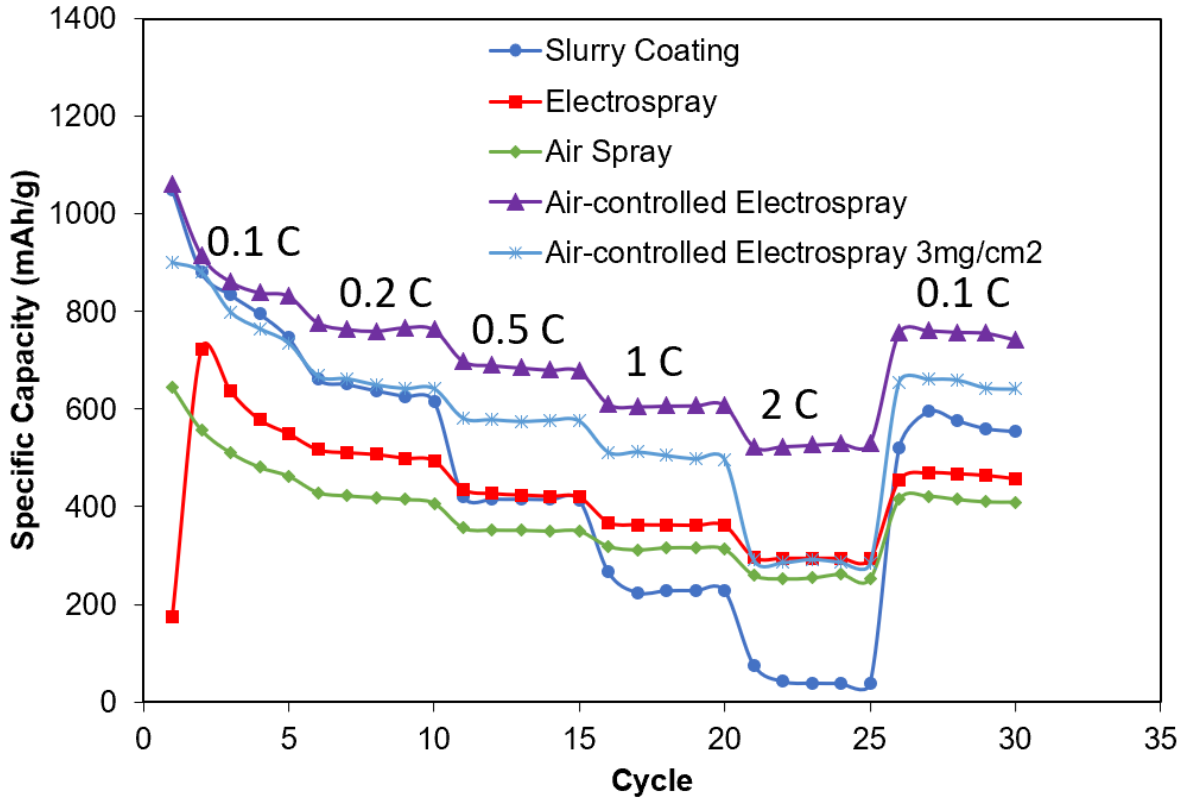

Fig. 2.10. Rate capability test for cells fabricated by slurry coating, electrospray, air spray and air-controlled electrospray

2.4. Conclusion

In summary, air-controlled electrospray is an excellent coating process that enables controlled morphology by changing parameters such as electric field and air pressure. Both increasing electric field strength and air pressure can contribute to decreasing droplet size and increasing number of droplets and results in different morphology and different electrochemical performance. After optimization, uniformly coated crack-free Li-S cathodes were obtained with porous micro-sized structures. These electrodes demonstrated improved capacity, retention and rate capability. The well-developed structure was efficient not only in providing conductive pathways for sulfur

utilization, but also for trapping polysulfides. In addition, the novel technique shows more potential and high stability at high loading.

Acknowledgment

This work was funded by Axium Nano, LLC (Cornell OSP No. 80674) and Department of Energy (DOE EERE Battery500). All the material characterizations were obtained via facilities at the Cornell Center for Materials Research (part of NSF MRSEC Program, Grant DMR 1120296).

REFERENCES

[1] A. Manthiram, Y. Fu, Y.-S. Su, Challenges and Prospects of Lithium–Sulfur Batteries, Acc. Chem. Res. 46 (2012) 1125–1134. doi:10.1021/ar300179v.

[2] N. Deng, W. Kang, Y. Liu, J. Ju, D. Wu, L. Li, B.S. Hassan, B. Cheng, A review on separators for lithiumsulfur battery: Progress and prospects, J. Power Sources. 331 (2016) 132–155. doi:10.1016/j.jpowsour.2016.09.044.

[3] A. Manthiram, Y. Fu, Y.-S. Su, Challenges and Prospects of Lithium-Sulfur Batteries, Acc. Chem. Res. (2012). doi:10.1021/ar300179v.

[4] L. Ji, M. Rao, H. Zheng, L. Zhang, Y. Li, W. Duan, J. Guo, E.J. Cairns, Y. Zhang, Graphene Oxide as a Sulfur Immobilizer in High Performance Lithium/Sulfur Cells, J. Am. Chem. Soc. 133 (2011) 18522–18525. doi:10.1021/ja206955k.

[5] S. Stankovich, D.A. Dikin, R.D. Piner, K.A. Kohlhaas, A. Kleinhammes, Y. Jia, Y. Wu, S.T. Nguyen, R.S. Ruoff, Synthesis of graphene-based nanosheets via chemical reduction of exfoliated graphite oxide, Carbon N. Y. 45 (2007) 1558–1565. doi:10.1016/j.carbon.2007.02.034.

[6] J.Q. Huang, T.Z. Zhuang, Q. Zhang, H.J. Peng, C.M. Chen, F. Wei, Permselective graphene oxide membrane for highly stable and anti-self-discharge lithium-sulfur batteries, ACS Nano. 9 (2015) 3002–3011. doi:10.1021/nn507178a.

[7] T. Wei, G. Luo, Z. Fan, C. Zheng, J. Yan, C. Yao, W. Li, C. Zhang, Preparation of graphene nanosheet/polymer composites using in situ reduction–extractive dispersion, Carbon N. Y. 47 (2009) 2296–2299. doi:10.1016/j.carbon.2009.04.030.

[8] X. Liang, C. Hart, Q. Pang, A. Garsuch, T. Weiss, L.F. Nazar, A highly efficient polysulfide mediator for lithium–sulfur batteries, Nat. Commun. 6 (2015). doi:10.1038/ncomms6682.

[9] A. Barinov, L. Gregoratti, P. Dudin, S. La Rosa, M. Kiskinova, Imaging and Spectroscopy of Multiwalled Carbon Nanotubes during Oxidation: Defects and Oxygen Bonding, Adv. Mater. 21 (2009) 1916–1920. doi:10.1002/adma.200803003.

[10] J. Guo, Y. Xu, C. Wang, Sulfur-impregnated disordered carbon nanotubes cathode for lithium-sulfur batteries, Nano Lett. 11 (2011) 4288–4294. doi:10.1021/nl202297p.

[11] J. Wang, Y. Yang, F. Kang, Porous carbon nanofiber paper as an effective interlayer for high-performance lithium-sulfur batteries, Electrochim. Acta. 168 (2015) 271–276. doi:10.1016/j.electacta.2015.04.055.

[12] M. Rao, X. Song, E.J. Cairns, Nano-carbon/sulfur composite cathode materials with carbon nanofiber as electrical conductor for advanced secondary lithium/sulfur cells, J. Power Sources. 205 (2012) 474–478. doi:10.1016/j.jpowsour.2012.01.047.

[13] B.P. Williams, Y.L. Joo, Tunable Large Mesopores in Carbon Nanofiber Interlayers for High-Rate Lithium Sulfur Batteries, J. Electrochem. Soc. 163 (2016) A2745–A2756. doi:10.1149/2.0931613jes.

[14] J. Lee, B. Ko, J. Kang, Y. Chung, Y. Kim, W. Halim, J.H. Lee, Y.L. Joo, Facile and scalable fabrication of highly loaded sulfur cathodes and lithium–sulfur pouch cells via air-controlled electrospray, Mater. Today Energy. 6 (2017) 255–263. doi:10.1016/j.mtener.2017.11.003.

[15] J. Song, T. Xu, M.L. Gordin, P. Zhu, D. Lv, Y.-B. Jiang, Y. Chen, Y. Duan, D. Wang, Nitrogen-Doped Mesoporous Carbon Promoted Chemical Adsorption of Sulfur and

Fabrication of High-Areal-Capacity Sulfur Cathode with Exceptional Cycling Stability for Lithium-Sulfur Batteries, Adv. Funct. Mater. 24 (2013) 1243–1250. doi:10.1002/adfm.201302631.

[16] Q. Pang, J. Tang, H. Huang, X. Liang, C. Hart, K.C. Tam, L.F. Nazar, A Nitrogen and Sulfur Dual-Doped Carbon Derived from Polyrhodanine@Cellulose for Advanced Lithium-Sulfur Batteries, Adv. Mater. 27 (2015) 6021–6028. doi:10.1002/adma.201502467.

[17] R. Fang, S. Zhao, P. Hou, M. Cheng, S. Wang, H.M. Cheng, C. Liu, F. Li, 3D Interconnected Electrode Materials with Ultrahigh Areal Sulfur Loading for Li-S Batteries, Adv. Mater. (2016). doi:10.1002/adma.201506014.

[18] H.J. Peng, D.W. Wang, J.Q. Huang, X.B. Cheng, Z. Yuan, F. Wei, Q. Zhang, Janus separator of polypropylene-supported cellular graphene framework for sulfur cathodes with high utilization in lithium-sulfur batteries, Adv. Sci. (2015). doi:10.1002/advs.201500268.

[19] C.P. Carroll, Y.L. Joo, Axisymmetric instabilities in electrospinning of highly conducting, viscoelastic polymer solutions, Phys. Fluids. (2009). doi:10.1063/1.3246024.

[20] Z.W. Seh, W. Li, J.J. Cha, G. Zheng, Y. Yang, M.T. McDowell, P.C. Hsu, Y. Cui, Sulphur-TiO 2 yolk-shell nanoarchitecture with internal void space for long-cycle lithium-sulphur batteries, Nat. Commun. 4 (2013). doi:10.1038/ncomms2327.

[21] P. Barai, A. Mistry, P.P. Mukherjee, Poromechanical effect in the lithium–sulfur battery cathode, Extrem. Mech. Lett. 9 (2016) 359–370. doi:10.1016/j.eml.2016.05.007.

[22] H. Shao, F. Ai, W. Wang, H. Zhang, A. Wang, W. Feng, Y. Huang, Crab shell-derived nitrogen-doped micro-/mesoporous carbon as an effective separator coating for high

energy lithium–sulfur batteries, J. Mater. Chem. A. 5 (2017) 19892–19900. doi:10.1039/C7TA05192A.

[23] F. Liu, Q. Xiao, H. Bin Wu, F. Sun, X. Liu, F. Li, Z. Le, L. Shen, G. Wang, M. Cai, Y. Lu, Regenerative Polysulfide-Scavenging Layers Enabling Lithium-Sulfur Batteries with High Energy Density and Prolonged Cycling Life, ACS Nano. (2017). doi:10.1021/acsnano.6b07603.

[24] Z. Sun, J. Zhang, L. Yin, G. Hu, R. Fang, H.-M. Cheng, F. Li, Conductive porous vanadium nitride/graphene composite as chemical anchor of polysulfides for lithium-sulfur batteries, 2017. doi:10.1038/ncomms14627.

[25] C. Fu, J. Guo, Challenges and current development of sulfur cathode in lithium–sulfur battery, Curr. Opin. Chem. Eng. 13 (2016) 53–62. doi:https://doi.org/10.1016/j.coche.2016.08.004.

[26] Y.S. Su, A. Manthiram, Lithium-sulphur batteries with a microporous carbon paper as a bifunctional interlayer, Nat. Commun. (2012). doi:10.1038/ncomms2163.

[27] S.H. Chung, A. Manthiram, Bifunctional separator with a light-weight carbon-coating for dynamically and statically stable lithium-sulfur batteries, Adv. Funct. Mater. (2014). doi:10.1002/adfm.201400845.

[28] X. Wang, Z. Wang, L. Chen, Reduced graphene oxide film as a shuttle-inhibiting interlayer in a lithium-sulfur battery, J. Power Sources. (2013). doi:10.1016/j.jpowsour.2013.05.063.

[29] L. Qie, C. Zu, A. Manthiram, A High Energy Lithium-Sulfur Battery with Ultrahigh-Loading Lithium Polysulfide Cathode and its Failure Mechanism, Adv. Energy Mater. 6 (2016) 1502459. doi:10.1002/aenm.201502459.

[30] C.H. Chang, S.H. Chung, A. Manthiram, Highly flexible, freestanding tandem sulfur cathodes for foldable Li-S batteries with a high areal capacity, Mater. Horizons. (2017). doi:10.1039/c6mh00426a.

[31] J. Yan, X. Liu, M. Yao, X. Wang, T.K. Wafle, B. Li, Long-Life, High-Efficiency Lithium-Sulfur Battery from a Nanoassembled Cathode, Chem. Mater. (2015). doi:10.1021/acs.chemmater.5b01780.

CHAPTER 3

Fabrication of Layer-on-Layer Sulfur Cathodes via Air-Controlled Electrospray

3.1 Introduction

Overuse of fossil fuels in the last centuries has accelerated the need for new, clean and sustainable energy sources to mediate severe energy and environmental issues. The lithium-ion battery is one of the methods for energy conversion and storage that is part of the solution. It is widely applied in many areas, including portable electronic devices, grid storage and electric vehicles. However, development of lithium-ion batteries has met its bottleneck. Rechargeable lithium sulfur batteries, which use sulfur and lithium as cathode and anode materials, respectively, are regarded as one of the promising substitutes for next generation energy storage systems. They have a high theoretical energy density (2600 Wh kg^{-1}) and a high theoretical energy capacity (1675 mA h g^{-1}) [1-4]. Moreover, the cathode active material, sulfur, is abundant, nontoxic, cost effective and environmentally friendly compared to materials in lithium-ion batteries.

However, despite its high theoretical energy density, there are a few problems that need to be solved to release its potential for use in real applications. The main problem is the shuttle effect, which results from dissolution of intermediate polysulfides species. The higher order polysulfides dissolve in electrolyte, pass through the separator to the anode, and directly react with lithium. This causes a series of issues, including loss of active materials, formation of an unstable solid electrolyte interface (SEI), and high resistance, and leads to fast capacity fading and poor rate capability. The insulating nature of sulfur and polysulfides also increase the cell resistance and the

difficulty of utilizing sulfur in electrochemical reactions. Last but not least, there is an 80% volume change from sulfur to Li_2S, which might passivate the reaction sites. [5,6].

Much progress has been made to address these issues in past decades. One of the most generally used methods is combining sulfur with conductive carbons, such as graphene oxide [4–6], , carbon nanotube [7,8], carbon nanofiber [9–12], or any functionalized carbon materials [13,14]. The various structures of carbon materials enhance the performance by increasing the conductivity and trapping polysulfides in the cathode through physical adsorption and/or chemical binding.

Application of an interlayer has been one of the popular solutions to use carbon materials to help prevent polysulfide shuttling [15–17]. The Manthiram group reported that highly conductive carbon interlayers can act as both a barrier to suppress the polysulfide shuttle effect and as an "additional current collector" to enhance the electrochemical performance[16]. Wang and co-workers also demonstrated the potential of using a reduced graphene interlayer and delivered a high initial discharge capacity of 1260 mAh g^{-1} [18].

Another challenging problem is how to maintain a good performance at high sulfur loading to achieve a high areal capacity. One of the simple but effective strategies for high performance sulfur batteries with excellent capacity and cycling is an intercalated cathode with layer-by-layer structure. It was first reported by Manthiram and co-workers [19]. By blade-casting pure sulfur between Al foil and a CNF layer, a high areal specific capacity of 19 mAh cm^{-2} was obtained with a loading over 14 mg cm^{-2}. Later, they further improved this method by stacking a tandem cell with multiple sulfur layers and carbon layers to an even higher sulfur loading at 16 mg cm^{-2} [20]. The layered structure not only makes it possible to fabricate a high loading nanostructure cathode, but also helps to mitigate shuttling effect by localizing polysulfides between layers and prolonging

their migration route. Li and co-workers also applied the similar layer structure strategy with PANI and CNT, obtaining remarkable results. [21]

In this chapter, we propose a solution for high loading lithium sulfur batteries by combining air-controlled electrospray and layer-on-layer technique. Applying the air-controlled electrospray technique enables an optimized sulfur layer coating with stable and porous structure that is favorable for active material utilization and shuttle effect mitigation. Meanwhile, the layer-on-layer strategy helps to improve the performance at high loading by trapping polysulfides locally between layers and prolong the migration route.

3.2 Experimental Methods

3.2.1 Preparation of Sulfur-Carbon solution

0.8 g of active sulfur material was mixed and grinded with 0.2 g of Ketjen Black. Then, the mixture was heat treated under air at 155^{o}C for 12 hours to ensure sulfur encapsulation in Ketjen Black. The KB/S mixture, graphene and polyacrylic acid were dispersed at 7:2:1 mass ratio in water and IPA at 7:3 volume ratio to have 6% solid content. The solution was sonicated at room temperature for one hour.

3.2.2 Coating of air-controlled electrospray sulfur layer

Lithium sulfur cathode solution was sprayed onto carbon coated aluminum foil using a coaxial needle (12-gauge inside, 16-gauge outside). The infusion rate and distance were kept at 0.05 ml min^{-1} and 10 cm, respectively. The voltage and air pressure were set up as 25 kV/ 15 psi.

3.2.3 Coating of air-controlled electrospray graphene layer

Graphene water solution (4 wt%) was sprayed using the same coaxial needle (12-gauge inside, 16-gauge outside). The infuse rate and distance were kept at 0.05 ml min and 20 cm, respectively. The voltage and air pressure were set up as 25 kV/ 25 psi.

3.2.3 Fabrication of cathodes

Li-S cathodes were fabricated by integrating air-controlled electrospray and layer-on-layer technique. One sulfur layer was sprayed at the bottom on carbon coated aluminum foil, and another graphene layer was spray on top. By this stacking, multi-layer cathodes, such as four-layer sulfur-graphene-sulfur-graphene electrodes, were able to be fabricated.

3.2.4 Electrolyte Composition

The electrolyte was 1 M of bis(trifluoromethane)sulfonimide lithium salt (LiTFSI) and 0.15 M of lithium nitrate ($LiNO_3$) in a 1:1 volume ratio of 1,2-dimethoxyethane (DME) and 1,3-Dioxolane (DOL). All were purchased from Sigma Aldrich.

3.2.5 Characterization Methods

Thermogravimetric analysis (TGA) was conducted on a TA Instruments Q500 with a rising temperature of 10 $^{o}C\ min^{-1}$ under nitrogen. Scanning electron microscopy (SEM) and Energy Dispersive X-ray (EDX) images were taken using a Tescan Mira3 FESEM.

Cathodes were assembled into 2032-type coin cells consisting of Li metal anodes (MTI Corporation) in an argon-filled glovebox. Cyclic voltammetry and electrochemical impedance spectroscopy (EIS) tests were performed using a potentiostat (BioLogic BCS 815). Cycling and rate capability test were carried out with a battery cycler (MTI Corporation) at room temperature.

3.3 Results and Discussion

The cathodes were fabricated by combining air-controlled electrospray and layer-on-layer technique as shown in Figure 3.1. Figure 3.2a shows the image of sulfur layer coating, which had uniform, porous surface with dark grey color. The graphene layer had smoother surface with light grey color as shown in Figure 3.2b.

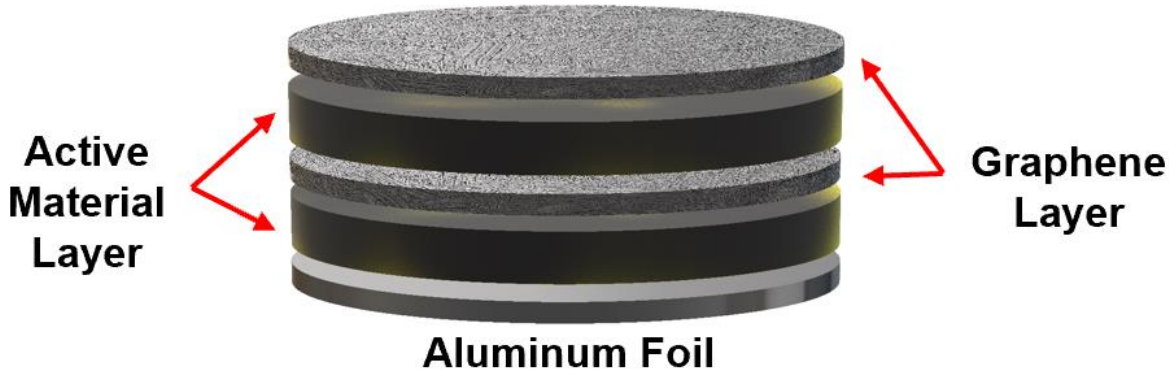

Fig. 3.1. Schematic illustration of cathode structure of layer-on-layer system

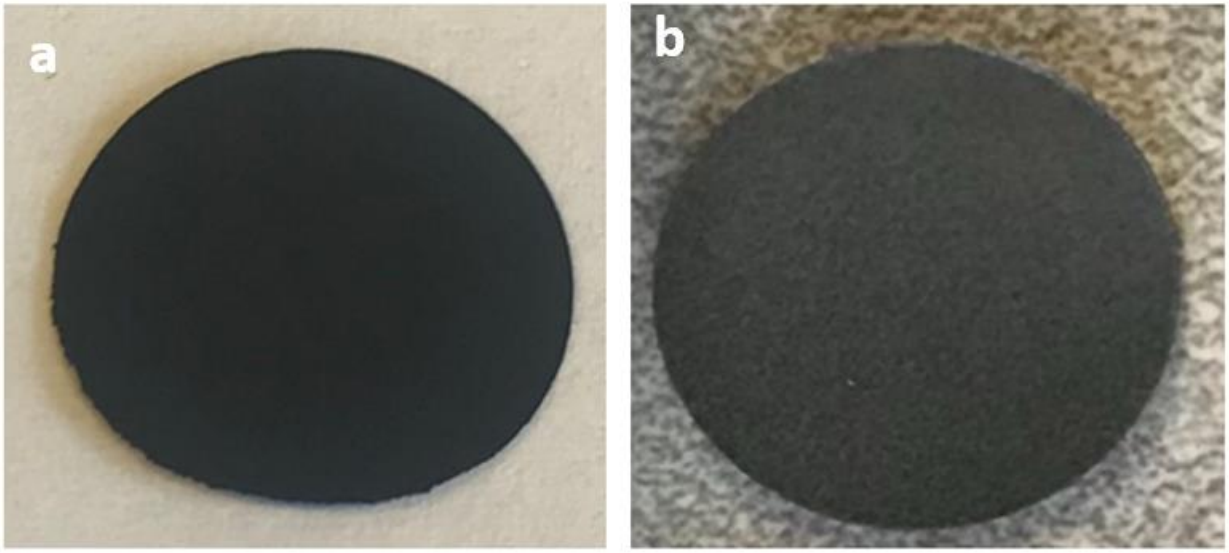

Fig. 3.2. image of a) active material layer b) graphene layer

Figure 3.3 presents the surface scanning electron microscopy (SEM) images and the corresponding elemental mapping results of the KB/S-Gr layer in layer-on-layer cathode before cycling. In the

KB/S-Gr active-material layer, the sulfur particles were homogeneously distributed. Ketjen Black provides micro porous structure for immobilizing the polysulfides and the conductive pathways for reducing resistance. The graphene conductive layer showed complete coverage of the sulfur layer beneath as shown in Figure 3.4. The thin layer of graphene can effectively retard the diffusion of polysulfides. Figure 3.5 shows the cross-section images of four-layer cathodes with thick graphene layers. Thanks to air-controlled electrospray, the porous sulfur layer had an intimate contact with the dense graphene layer.

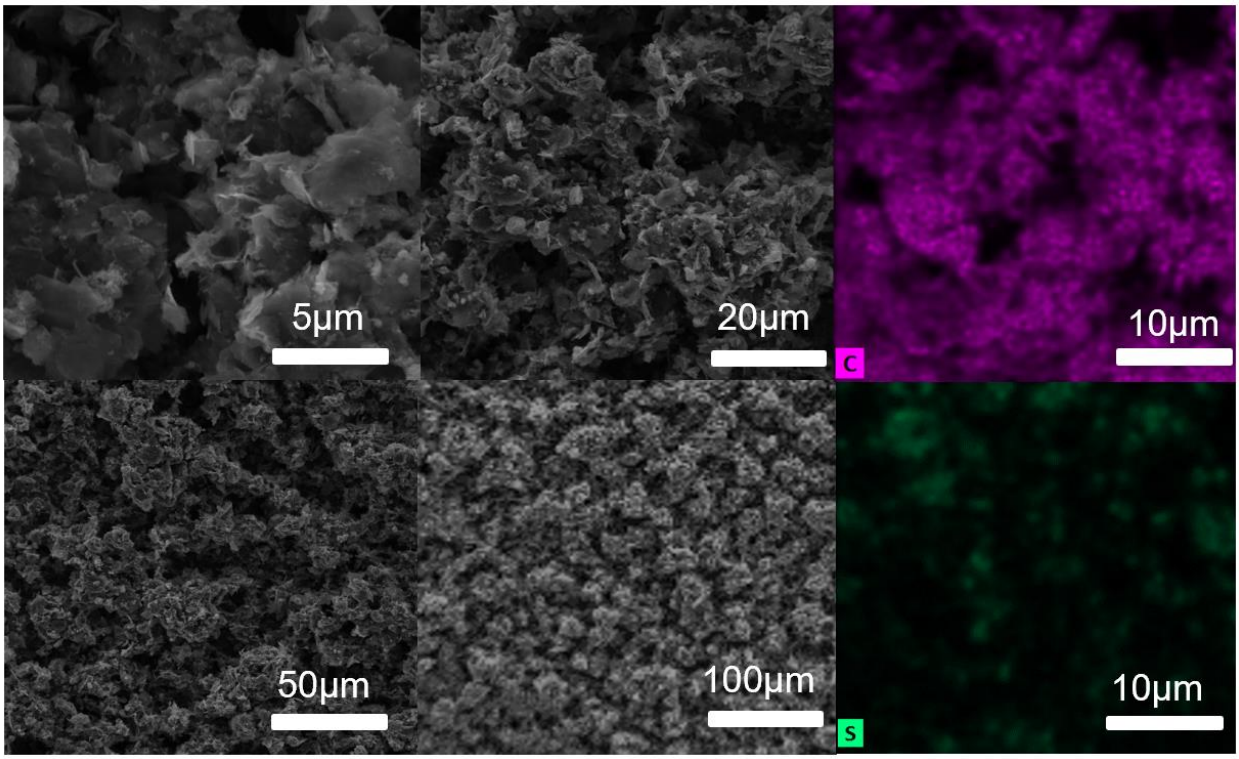

Fig. 3.3. SEM images and corresponding elemental mapping for active material layer

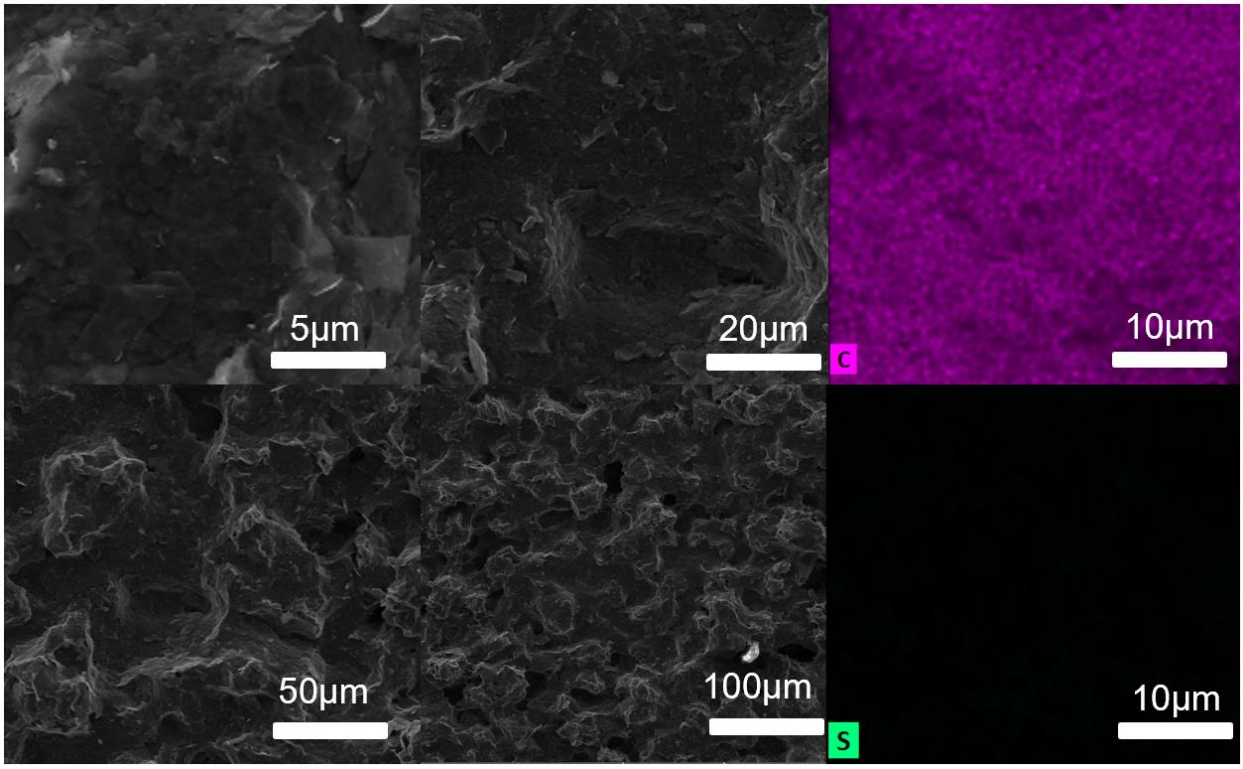

Fig. 3.4. SEM images and corresponding elemental mapping for graphene layer

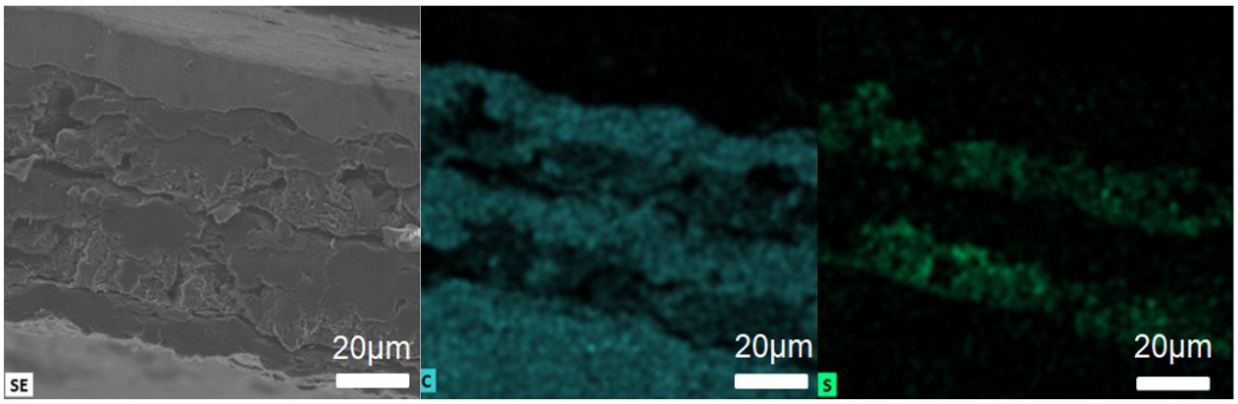

Fig. 3.5. SEM images and corresponding elemental mapping for cross-section image of layer-on-layer (4 layers) system

Electrochemical impedance spectroscopy (EIS) results were obtained for air-controlled electrospray, and layer-on-layer electrodes with different thickness coating of graphene layer. At the medium to high frequency region of the Nyquist plot, a depressed semicircle can be interpreted as the bulk resistance of electrolyte and charge transfer resistance. According to Figure 3.6, the air-controlled electrospray cathode had the highest resistance. This can be explained by the higher amount of highly conductive graphene in the layer-on-layer electrodes. Meanwhile, the thicker the graphene layer, the lower the resistance. At the low frequency region, an oblique line tells the diffusion lithium ions[22]. The dense graphene layer largely hindered the ion diffusion, which resulted in the lowest slope and worst diffusion in the layer-on-layer electrode with thick graphene layer.

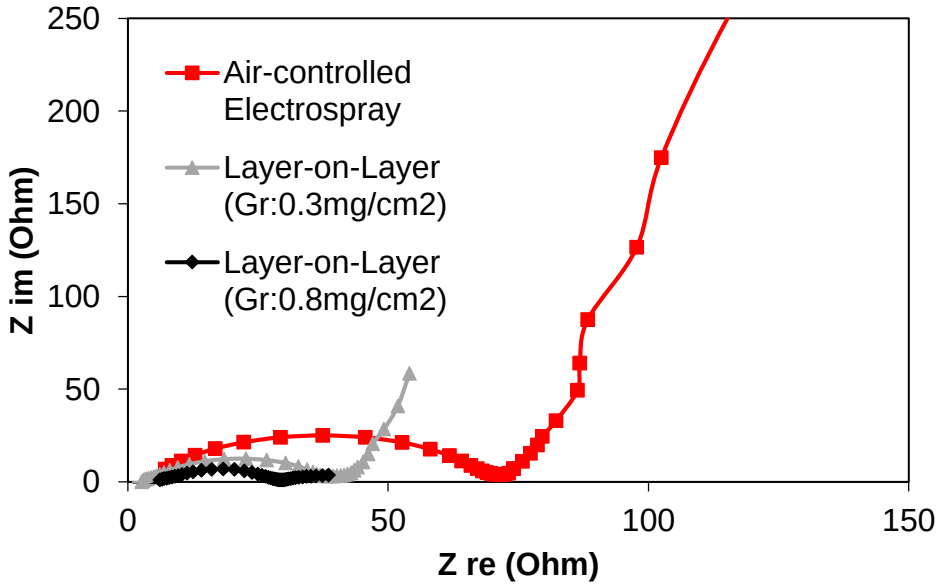

Fig. 3.6. EIS characterization on air-controlled electrospray and layer-on-layer cathodes with different thickness of graphene layer

Cyclability tests were conducted at a 0.2 C rate for conventional one-layer air-controlled electrospray, two-layer and four-layer cathodes. Results were presented in Figure 3.7. At the sulfur loading of 1mg cm^{-2}, layer-on-layer electrodes already showed improved capacities over the air-

controlled electrospray electrodes. More importantly, the additional graphene layer effectively trapped polysulfides and made a big difference in cycle life, where two-layer and four-layer electrodes exhibits a better capacity retention after 100 cycles. The advantage of layer-on-layer structure was further emphasized at higher loading. At a loading of 3 mg cm^{-2}, the superb performance still maintained. Due to the difficulty in ion diffusion from graphene layer, it took nearly 20 cycles for the cell to be fully activated and exhibit a high capacity of 868.1 mAh g^{-1} after running for 100 cycles. Voltage profile at 5^{th} cycle was plotted in Figure.3.8 to explore their behavior difference. All cells, except for the high sulfur loading one, showed well defined plateau. One difference is that, without layer of graphene, air-controlled electrospray cell showed a larger overpotential due to less conductivity. The Layer-on-Layer cell was still in activation at this time, it had a short and fast-decreasing second plateau, which indicated problem in further conversion to insoluble long chain polysulfide with inadequate reaction sites.

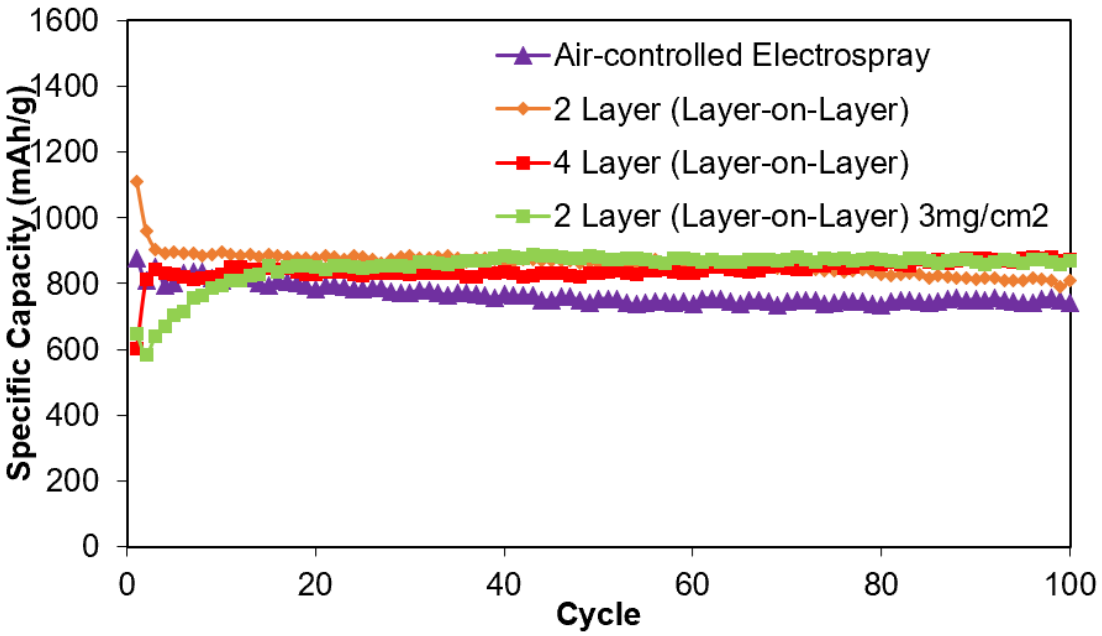

Fig. 3.7. Cycling performance for cells fabricated by air-controlled electrospray and layer-on-layer cells

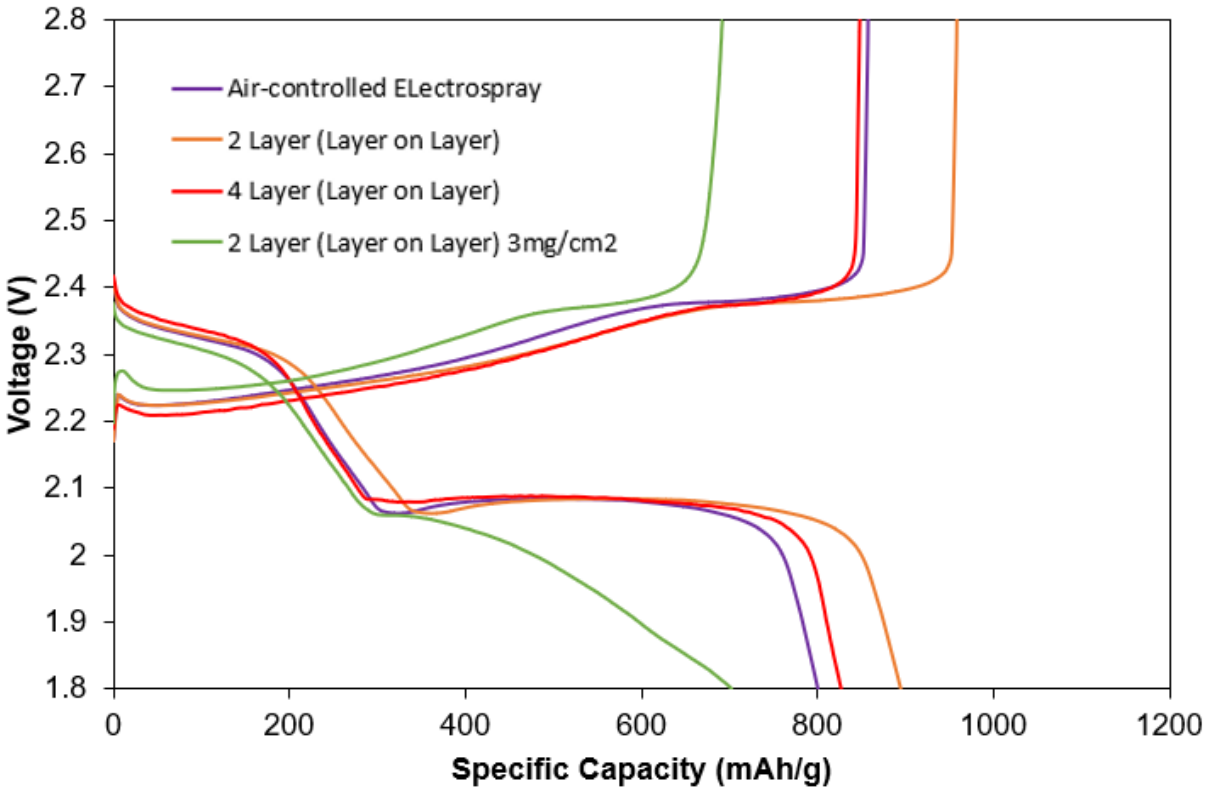

Fig. 3.8. Voltage profile of air-controlled electrospray and Layer-on-Layer cells

The rate capability test was also carried out at different current densities for one-layer air-controlled electrospray and layer-on-layer (2 layers) electrodes at a loading of 1mg cm^{-2} as shown in Figure 3.9. As expected, the layer-on-layer cell shower a high discharge capacity at a relatively low C rate. Even when the current density increased to 1 C, the cell with layer-on-layer structure still maintained 67.0 % of its initial capacity, whereas it was 57.5% for the one-layer cell. However, at 2 C, the result was completely different, the capacity retention for the two-layer and one-layer cells were 37.6% and 49.3% respectively. This can be explained by the limit of ion diffusion due to the dense graphene layer, as discussed with EIS.

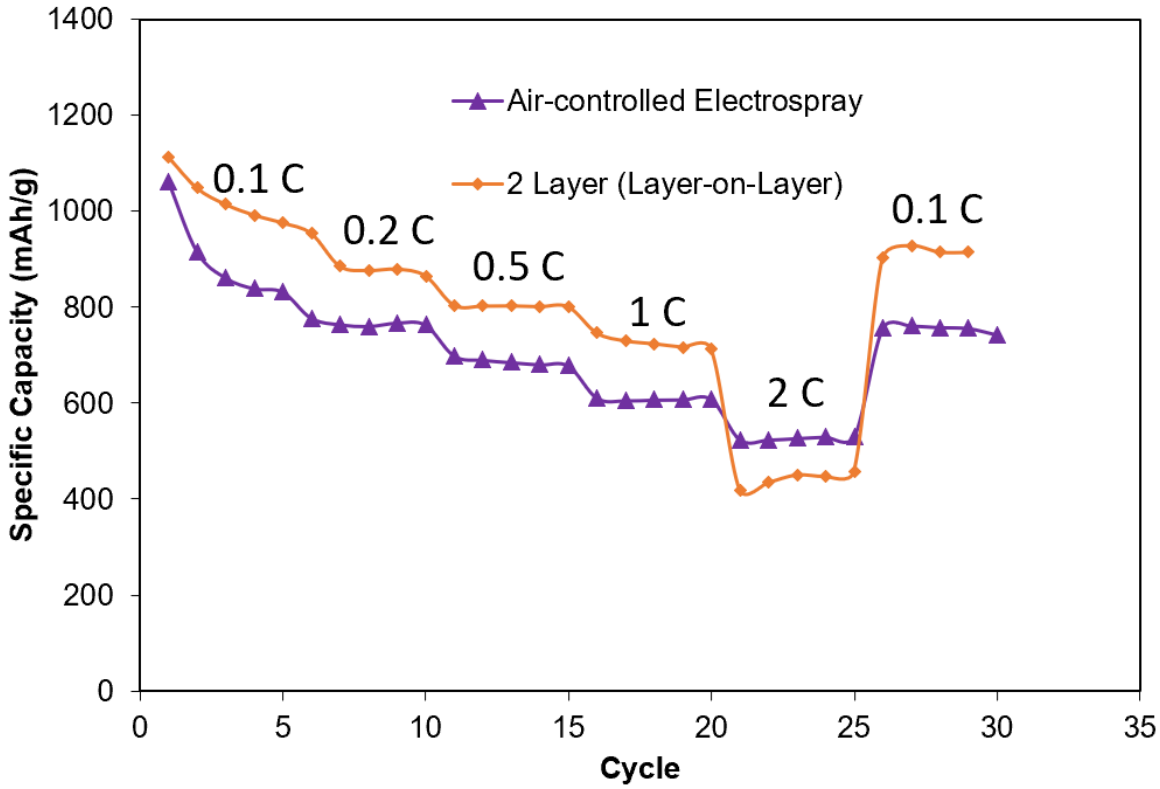

Fig. 3.9. Cycling performance for cells fabricated by air-controlled electrospray and layer-on-layer cells

After cycling finished, the cells were dissembled, and SEM and EDS analysis was carried out on the anode side. As shown in Figure 3.10, lithium metal of the one-layer cathodes had severe dendrite issues, which indicates a higher extent of side-reactions due to higher concentration of polysulfides migrating through the separator from the cathode. On the contrary, with the coating of graphene, the shuttling effect was less severe and polysulfides were successfully trapped locally.

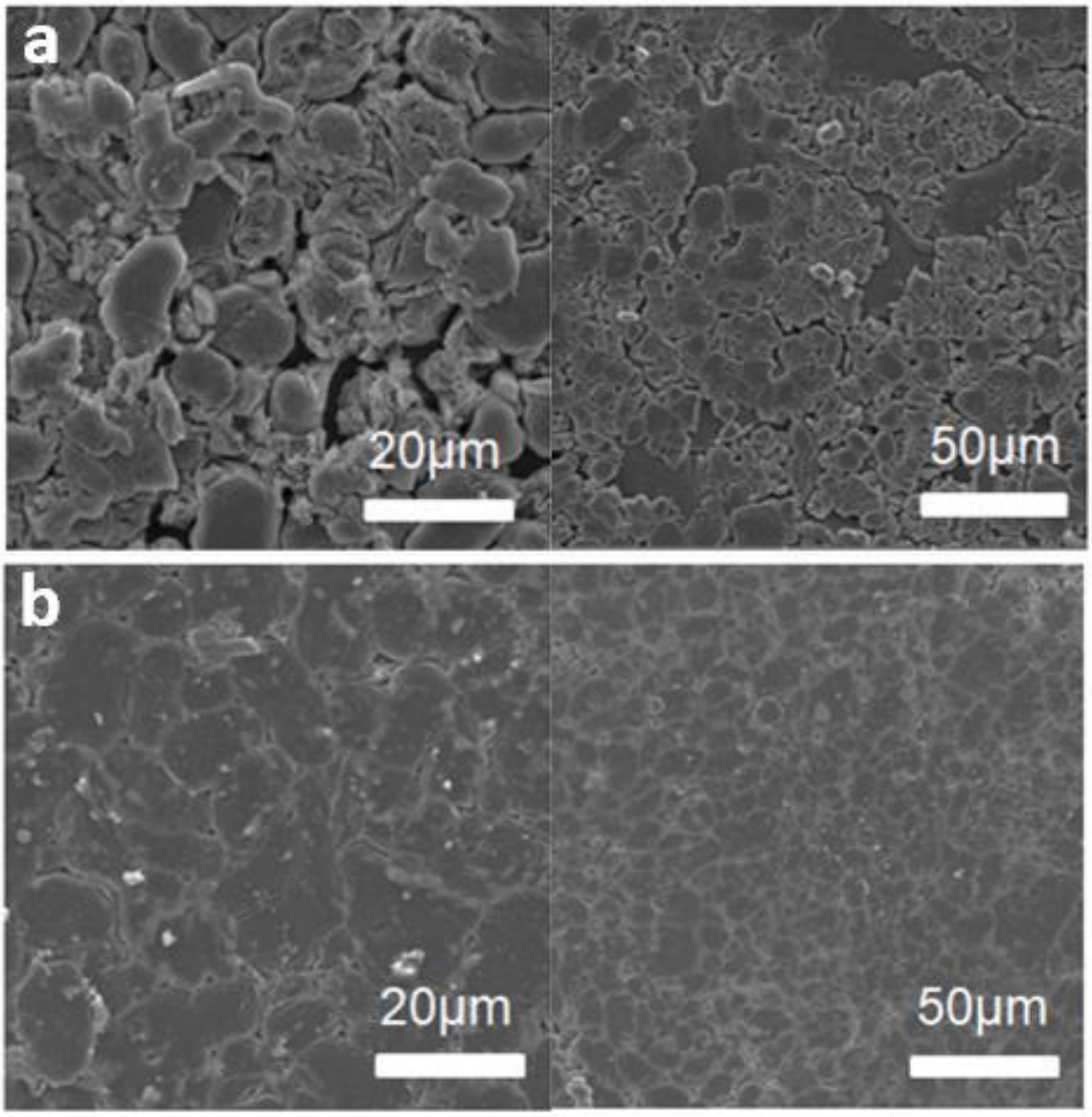

Fig. 3.10. SEM image of the anodes after cycling for a) air-controlled electrospray and b) layer-on-layer cell

3.4. Conclusion

In conclusion, by combining air-controlled electrospray and the layer-on-layer technique, a facile process was used to fabricate Li-S cathodes for high sulfur loading. The graphene layer not only acted as an additional current collector to increase the conductivity and improve sulfur utilization, but also worked as part of the layer structure for local polysulfide trapping and mitigation of the

shuttle effect. However, one issue needing to be further addressed is that thick and dense graphene layers can negatively influence ion diffusion in the cathode and worsen cell performance at high current densities. Thus, future work needs to be done to optimize the layer-on-layer structure deposited by air-controlled electrospray.

Acknowledgment

This work was funded by Axium Nano, LLC (Cornell OSP No. 80674) and Department of Energy (DOE EERE Battery500). All the material characterizations were obtained via facilities at the Cornell Center for Materials Research (part of NSF MRSEC Program, Grant DMR 1120296).

REFERENCES

[1] A. Manthiram, Y. Fu, Y.-S. Su, Challenges and Prospects of Lithium–Sulfur Batteries, Acc. Chem. Res. 46 (2012) 1125–1134. doi:10.1021/ar300179v.

[2] N. Deng, W. Kang, Y. Liu, J. Ju, D. Wu, L. Li, B.S. Hassan, B. Cheng, A review on separators for lithiumsulfur battery: Progress and prospects, J. Power Sources. 331 (2016) 132–155. doi:10.1016/j.jpowsour.2016.09.044.

[3] A. Manthiram, Y. Fu, Y.-S. Su, Challenges and Prospects of Lithium-Sulfur Batteries, Acc. Chem. Res. (2012). doi:10.1021/ar300179v.

[4] L. Ji, M. Rao, H. Zheng, L. Zhang, Y. Li, W. Duan, J. Guo, E.J. Cairns, Y. Zhang, Graphene Oxide as a Sulfur Immobilizer in High Performance Lithium/Sulfur Cells, J. Am. Chem. Soc. 133 (2011) 18522–18525. doi:10.1021/ja206955k.

[5] S. Stankovich, D.A. Dikin, R.D. Piner, K.A. Kohlhaas, A. Kleinhammes, Y. Jia, Y. Wu, S.T. Nguyen, R.S. Ruoff, Synthesis of graphene-based nanosheets via chemical reduction of exfoliated graphite oxide, Carbon N. Y. 45 (2007) 1558–1565. doi:10.1016/j.carbon.2007.02.034.

[6] J.Q. Huang, T.Z. Zhuang, Q. Zhang, H.J. Peng, C.M. Chen, F. Wei, Permselective graphene oxide membrane for highly stable and anti-self-discharge lithium-sulfur batteries, ACS Nano. 9 (2015) 3002–3011. doi:10.1021/nn507178a.

[7] A. Barinov, L. Gregoratti, P. Dudin, S. La Rosa, M. Kiskinova, Imaging and Spectroscopy of Multiwalled Carbon Nanotubes during Oxidation: Defects and Oxygen Bonding, Adv. Mater. 21 (2009) 1916–1920. doi:10.1002/adma.200803003.

[8] J. Guo, Y. Xu, C. Wang, Sulfur-impregnated disordered carbon nanotubes cathode for lithium-sulfur batteries, Nano Lett. 11 (2011) 4288–4294. doi:10.1021/nl202297p.

[9] J. Wang, Y. Yang, F. Kang, Porous carbon nanofiber paper as an effective interlayer for high-performance lithium-sulfur batteries, Electrochim. Acta. 168 (2015) 271–276. doi:10.1016/j.electacta.2015.04.055.

[10] M. Rao, X. Song, E.J. Cairns, Nano-carbon/sulfur composite cathode materials with carbon nanofiber as electrical conductor for advanced secondary lithium/sulfur cells, J. Power Sources. 205 (2012) 474–478. doi:10.1016/j.jpowsour.2012.01.047.

[11] B.P. Williams, Y.L. Joo, Tunable Large Mesopores in Carbon Nanofiber Interlayers for High-Rate Lithium Sulfur Batteries, J. Electrochem. Soc. 163 (2016) A2745–A2756. doi:10.1149/2.0931613jes.

[12] J. Lee, B. Ko, J. Kang, Y. Chung, Y. Kim, W. Halim, J.H. Lee, Y.L. Joo, Facile and scalable fabrication of highly loaded sulfur cathodes and lithium–sulfur pouch cells via air-controlled electrospray, Mater. Today Energy. 6 (2017) 255–263. doi:10.1016/j.mtener.2017.11.003.

[13] J. Song, T. Xu, M.L. Gordin, P. Zhu, D. Lv, Y.-B. Jiang, Y. Chen, Y. Duan, D. Wang, Nitrogen-Doped Mesoporous Carbon Promoted Chemical Adsorption of Sulfur and Fabrication of High-Areal-Capacity Sulfur Cathode with Exceptional Cycling Stability for Lithium-Sulfur Batteries, Adv. Funct. Mater. 24 (2013) 1243–1250. doi:10.1002/adfm.201302631.

[14] Q. Pang, J. Tang, H. Huang, X. Liang, C. Hart, K.C. Tam, L.F. Nazar, A Nitrogen and Sulfur Dual-Doped Carbon Derived from Polyrhodanine@Cellulose for Advanced Lithium-Sulfur Batteries, Adv. Mater. 27 (2015) 6021–6028.

doi:10.1002/adma.201502467.

[15] C. Fu, J. Guo, Challenges and current development of sulfur cathode in lithium–sulfur battery, Curr. Opin. Chem. Eng. 13 (2016) 53–62. doi:https://doi.org/10.1016/j.coche.2016.08.004.

[16] Y.S. Su, A. Manthiram, Lithium-sulphur batteries with a microporous carbon paper as a bifunctional interlayer, Nat. Commun. (2012). doi:10.1038/ncomms2163.

[17] S.H. Chung, A. Manthiram, Bifunctional separator with a light-weight carbon-coating for dynamically and statically stable lithium-sulfur batteries, Adv. Funct. Mater. (2014). doi:10.1002/adfm.201400845.

[18] X. Wang, Z. Wang, L. Chen, Reduced graphene oxide film as a shuttle-inhibiting interlayer in a lithium-sulfur battery, J. Power Sources. (2013). doi:10.1016/j.jpowsour.2013.05.063.

[19] L. Qie, C. Zu, A. Manthiram, A High Energy Lithium-Sulfur Battery with Ultrahigh-Loading Lithium Polysulfide Cathode and its Failure Mechanism, Adv. Energy Mater. 6 (2016) 1502459. doi:10.1002/aenm.201502459.

[20] C.H. Chang, S.H. Chung, A. Manthiram, Highly flexible, freestanding tandem sulfur cathodes for foldable Li-S batteries with a high areal capacity, Mater. Horizons. (2017). doi:10.1039/c6mh00426a.

[21] J. Yan, X. Liu, M. Yao, X. Wang, T.K. Wafle, B. Li, Long-Life, High-Efficiency Lithium-Sulfur Battery from a Nanoassembled Cathode, Chem. Mater. (2015). doi:10.1021/acs.chemmater.5b01780.

[22] H. Shao, F. Ai, W. Wang, H. Zhang, A. Wang, W. Feng, Y. Huang, Crab shell-derived nitrogen-doped micro-/mesoporous carbon as an effective separator coating for high

energy lithium–sulfur batteries, J. Mater. Chem. A. 5 (2017) 19892–19900. doi:10.1039/C7TA05192A.

Chapter 4

Current Collector Free and High Gravimetric Energy Density of Lithium Sulfur Battery via Air-controlled Electrospray Process

4.1 Introduction

Amid the rapid development of technology, the demands of energy storage have been increasing exponentially. The current commercial lithium-ion battery has approached its limit. One promising candidate for the next generation of energy storage is the lithium sulfur (Li-S) battery [1,2]. Li-S battery technology has been gaining momentum due to its high theoretical energy density and low cost. However, setbacks including active material dissolution, shuttle effect, and insulating sulfur materials hinder the technology commercialization [3,4].

Many approaches have been conducted to improve the overall energy density and prolong the cycle life of lithium-sulfur. One of the most popular approaches is infusing sulfur materials into a porous carbon structure [5]. Carbon is cheap and provides an excellent conduit for electron transfer to improve sulfur utilization. Other investigations have been focused on modifying the mechanical and chemical structures of the electrode and separator. Several examples of physical approaches are implementing a porous carbon network structure as a cathode [6], embedding carbon nanofiber as an interlayer [7], coating the separator with carbon [8], and tuning the pore distribution within the carbon network to provide more access for diffusion of lithium-ion and suppress the migration of intermediate species [9]. Examples of chemical approaches include chemically adding functional groups or electronegative components, such as graphene oxide [10,11], cobalt disulfide [12], and titanium oxide [13], to either repel or absorb the polysulfides and suppress their diffusion, consequently prolonging retention and improving capacity.

In this work, we employed a unique method to improve the overall gravimetric energy density by eliminating the metal current collector, thereby lowering the overall cell cost. Previously, we reported a binder-free and instant dry process for lithium-ion battery electrode fabrication [14]. Here, we apply a similar process for the lithium-sulfur system. Previous literature observed that by adhering the active material directly onto the separator, higher capacity could be achieved mainly due to the removal of binder and 3D morphology generated by vacuum filtration [15]. We developed the current-collector free concept for lithium-sulfur batteries by using an air-controlled electrospray process to deposit material directly onto the separator.

Graphene was electrosprayed onto a Celgard separator to improve the electrical conductivity and suppress polysulfide diffusion [16]. Afterwards, active materials were directly electrosprayed onto the graphene coated separator, thus eliminating the current collector that contributes more than 50% of the total electrode weight for an active material loading below 4.34 mg cm^{-2}. The air-controlled electrospray process induces fast solvent evaporation due to the drag force from the air that impinges the droplets, leaving dry solute on the target [17]. The schematic and digital images of the air-controlled electrospray process on both a current collector and polymer separator are depicted in Figure 4.1 below.

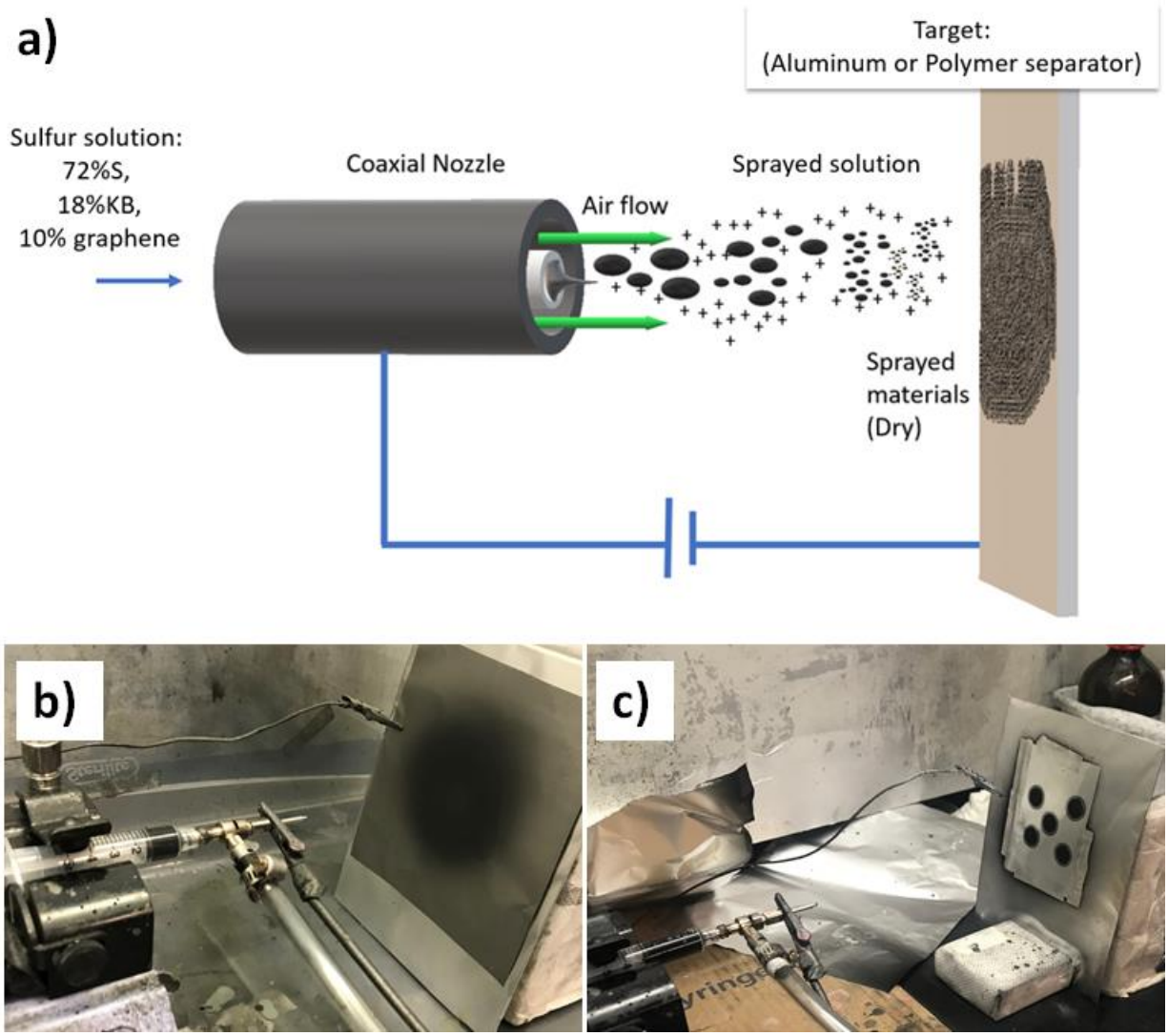

Fig. 4.1. **a)** Schematic illustration of air-controlled electrospray process for active material deposition **b)** Deposition of active materials onto aluminum current collector **c)** Deposition of active materials onto graphene coated separator.

4.2 Materials and Methods

4.2.1 Preparation of the active material solution

For the active material, 0.072 g of sulfur was mixed with 0.018 g of Ketjen Black (AkzoNobel). The mixture was then heat treated at 155^{o}C for 12 hours to ensure sulfur infiltration. Afterward,

100 mg of 10 wt% graphene solution (ACS Nano) was added to the mixture. The final composition of sulfur:Ketjen Black:graphene was about 72:18:10. Finally, the mixture was dispersed in 5 ml water and isopropanol solvent at 8:2 v/v ratio.

4.2.2 Fabrication of graphene coated separator

First, 5 ml of the 10% wt of graphene solution(ACS nano) was diluted to 4 wt% in water. Then, the diluted solution was deposited onto the Celgard separator with air-controlled electrospraying. The electrospraying conditions are as follows: 25 kV applied voltage, 10 cm distance from the nozzle tip to the collector, 12 psi convective airflow rate, and 0.1 ml min^{-1} solution pump rate. After the Celgard separator was uniformly coated with a graphene layer, it was punched into 20 mm diameter disks. Typical graphene coating was around 0.2 – 0.4 mg cm^{-2}.

4.2.3 Active material deposition onto the aluminum current collector

Similarly, 5 ml of sulfur-carbon solution from step 2.1 was sprayed onto the aluminum current collector for the reference cell. The voltage applied was 25 kV, distance from the nozzle tip to current collector was 12 cm, convective airflow rate was 10 psi, and solution pump rate was 0.1 ml min^{-1}. After deposition, the electrode was punched into 17.5 mm diameter disks. Typical active sulfur loading was around 0.6 – 0.8 mg cm^{-2} and the content was around 72% as measured by the TGA.

4.2.4 Active material deposition onto celgard separator

Polyethylene terephthalate (PET) film with previously punched electrode sized holes was placed on top of the punched disks of coated separators to immobilize the target and direct the active material deposition to the center. Electrospraying conditions were similar to those used for the reference electrodes above.

4.2.5 Electrolyte Composition

The electrolyte was 1 M of bis(trifluoromethane)sulfonimide lithium salt (LiTFSI) and 0.1 M of lithium nitrate ($LiNO_3$) in a 1:1 volume ratio of 1,2-dimethoxyethane (DME) and 1,3-Dioxolane (DOL). All were purchased from Sigma Aldrich.

4.2.6 Characterization Methods

Thermogravimetric analysis was carried out with a TA Instruments Q500 at a heating rate of 10 $^oC\ min^{-1}$ under an N_2 atmosphere. X-ray diffraction analysis was conducted with a Bruker D8 Advance ECO powder diffractometer from 10^o to 80^o at a scan rate of $0.1^o\ s^{-1}$. Scanning electron microscopy (SEM) images were taken using a Tescan Mira3 FESEM. Electrochemical characterizations of the coated separator were performed using 2032-type coin cells consisting of Li metal anodes (MTI Corporation). All cells were assembled in an argon-filled glove box. Cyclic voltammetry and electrochemical impedance spectroscopy (EIS) tests were performed using a potentiostat (BioLogic BCS 815). Galvanostatic charge/discharge cycles were carried out in the voltage range of 1.8-2.8 V using a battery cycler (MTI Corporation) at room temperature. All current densities, specific discharge capacities, and rate capability are calculated in this study were based on sulfur mass. Gravimetric discharge capacity is calculated based on the total material mass on the cathode side.

4.3 Results and Discussion

Images of active material on both the aluminum current collector (S-Al) and graphene-coated separator (S-Sep) are presented in Figure 4.2a below. The grey color of the separator shows that graphene uniformly covers its entire surface. It has been previously shown that a carbon coated separator improves the electrical conductivity and suppresses polysulfide diffusion [8]. For the

configuration in this work, graphene was used to provide a flat surface for active sulfur material deposition. The schematic illustration of both systems is shown in Figure 4.2b & 4.2c below. The reference cell S-Al system is also tested with a graphene-coated separator to provide a fair comparison of both systems. The S-Sep system is bendable (Figure 4.2d,e) and preserves its structure even after bending, which offers potential for future flexible substrate applications.

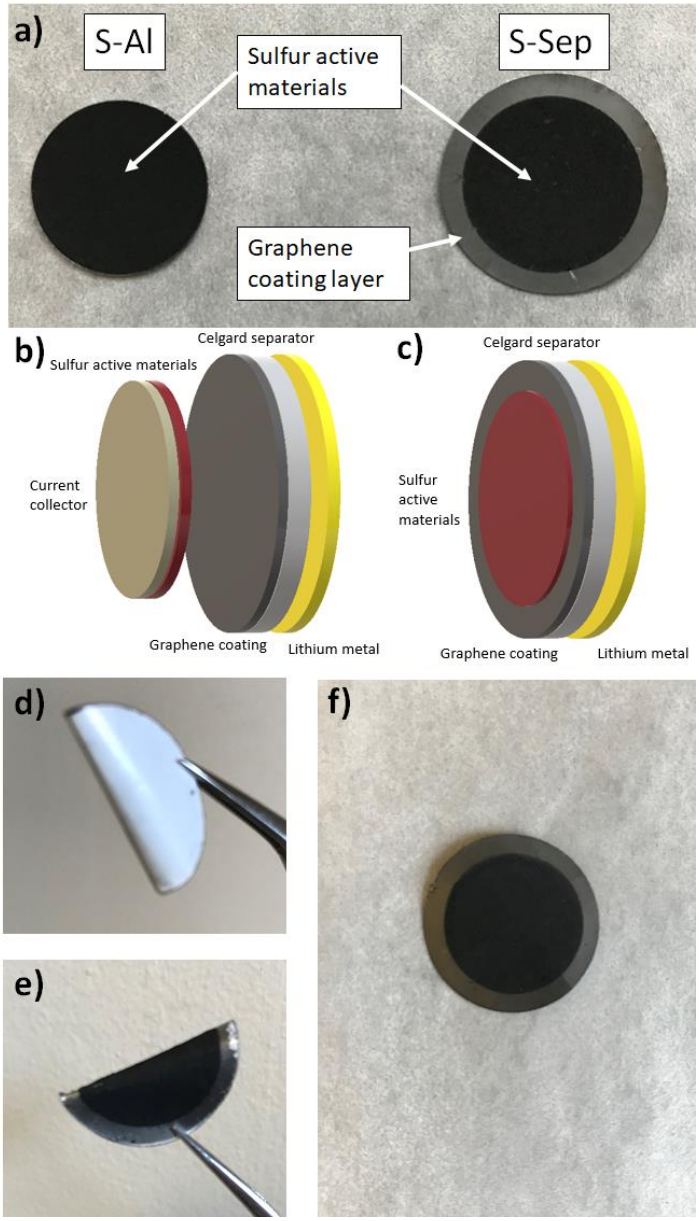

Fig. 4.2. **a)** Digital image of S-Al (left) and S-Sep (right). **b)** Schematic illustrations of S-Al and **c)** S-Sep for our systems **d,e)** Flexible S-Sep cathode during bending and **f)** after bending.

The SEM images of both systems are displayed in Figure 4.3a-d below. From the cross-sectional images (Figure 4.3a,b), continuous and smooth transition layers of sulfur active materials with either the metal current collector or Celgard separator are observed. Unfortunately, the graphene layer of S-Sep is unable to be seen because of its extremely thin structure (on the order of nanometers). The interface between active material and coated separator will be different for both S-Al and S-Sep configurations in the assembled cell. For the S-Al system, there will be a discontinuous interface between the sulfur active material and separator due to them simply being compressed together. The presence of electrolyte might also form a thin layer between the separator and the cathode, which might increases the overall cell resistance. However, in the S-Sep system a continuous interface between active material and graphene-coated separator was established due to the direct deposition of the active material. In the top-view SEM images (Figure 4.3c,d), both systems show a porous morphology as a result of the spraying process. Having a porous mechanical structure is very beneficial in the sulfur battery, because it enhances electrolyte wetting and consequently improves sulfur utilization [18]. X-ray diffraction (XRD) was used to characterize some features of S-Al and S-Sep (Figure 4.3e). Both systems exhibit a distinguished peak at 27^{o}, which corresponds to a graphitic peak from the presence of graphene in the system [19]. Lastly, the circle and rectangle peaks correspond to celgard separator and aluminum current collector, respectively [20,21].

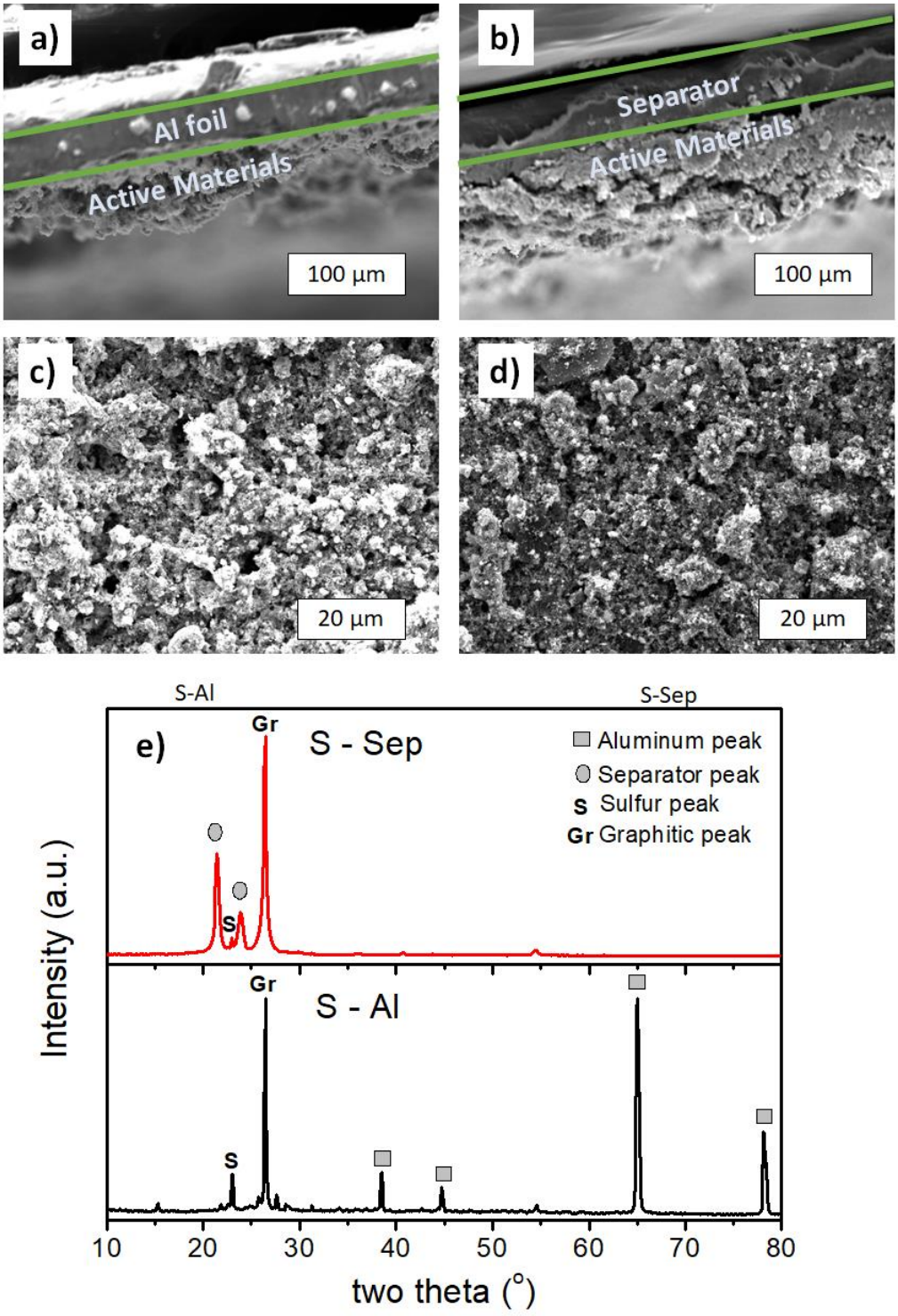

Fig. 4.3. Cross-section SEM images of **a)** S-Al and **b)** S-Sep systems. Top view SEM images of **c)** S-Al and **d)** S-Sep SEM images. **e)** XRD characterization on S-Al and S-Sep systems.

To check the consistency of sulfur content after spraying, the active materials were scraped from the aluminum collector for thermogravimetric analysis (TGA). From the S-Al TGA spectrum (Figure 4.4a), the sprayed sulfur content was around 75%, which was 3% higher than the original composition. Fast evaporation from the convective dry air causes a slight carbon loss during the spray process. Ketjen black and graphene are very light materials, and easily blown away. Based on the electrochemical impedance spectroscopy (EIS) in Figure 4.4b, the S-Sep system shows a smaller semicircle width than that of S-Al, which corresponds to lower charge transfer resistance. This might be due to excellent contact between active materials and graphene-coated separator and/or elimination of aluminum current collector. On the other hand, rough morphology from S-Al might result in poor contact between active materials and separator, leading to the higher resistance.

Cyclic voltammogram (CV) profiles of S-Al and S-Sep are presented in Figures 3.4c and 3.4d, respectively, to evaluate the electrochemical performance between the two systems. Both curves exhibit two reduction peaks at 2.3V and 2.0V, which dictate the reductions of higher order and lower order polysulfides, respectively. An oxidation peak at around 2.4V refers to the formation of sulfur particles [22]. Both CV profiles show a polarization effect that may be attributed to a relatively high content of sulfur, which requires significant energy to reduce it. On the first cycle, S-Al shows a small peak for the lower order polysulfide reaction whereas in S-Sep does not. One possible explanation is that the porous mechanical structure of S-Al has a higher exposed surface area for the sulfur-electrolyte interface. In the case of the S-Sep system, a dense surface between the sulfur/separator interface causes more difficult electrolyte penetration, and ultimately results in less reaction sites and sluggish kinetic for the first cycle.

To evaluate battery cell performance, cyclability tests were carried out at a 0.25C rate . Sulfur loading in both systems was around 1 – 1.2 mg in total. Based on Figure 4.4e below, both systems show a similar specific capacity performance. It implies that although S-Sep possesses lower electrical resistance, S-Al has more ionic accessibility because of its rough and porous structure facing the separator. When comparing specific capacity (Figure 4.4e), S-Al shows a very close performance compared to S-Sep, which is expected since they have similar composition and chemistry. S-Al and S-Sep exhibit initial capacities at 1220 mAh g^{-1} and 1141 mAh g^{-1}, respectively. After 100 cycles, S-Al and S-Sep show final discharge capacities at 658 mAh g^{-1} and 663 mAh g^{-1}, respectively. However, the distinction between the two systems can be seen clearly by looking at their gravimetric capacity (Figure 4.4f). Instead of calculating by mass of sulfur material, the total capacity was divided by the total material mass on the cathode side: sulfur, carbon, and, if present, the aluminum current collector. S-Al shows an initial gravimetric capacity of only 138 mAh g^{-1}, whereas S-Sep shows an initial capacity at 821 mAh g^{-1}. S-Sep shows a reversible gravimetric capacity at around 600 mAh g^{-1} and S-Al shows a gravimetric capacity at around 100 mAh g^{-1}. The presence of aluminum contributes to more than 50% of total mass on the cathode side, especially when sulfur loading is relatively low (below 3 mg cm^{-2}).

Rate capability shown in Figure 4.4g illustrates consistent behavior with the cycling performance for both systems, despite them having high sulfur content (~75 %). Both systems show a similar discharge capacity at different rates. Even at 2C, both samples show capacity at around 450 mAh g^{-1}. By directly depositing active materials onto the separator via an air-controlled electrospray process, high gravimetric energy density batteries can be obtained.

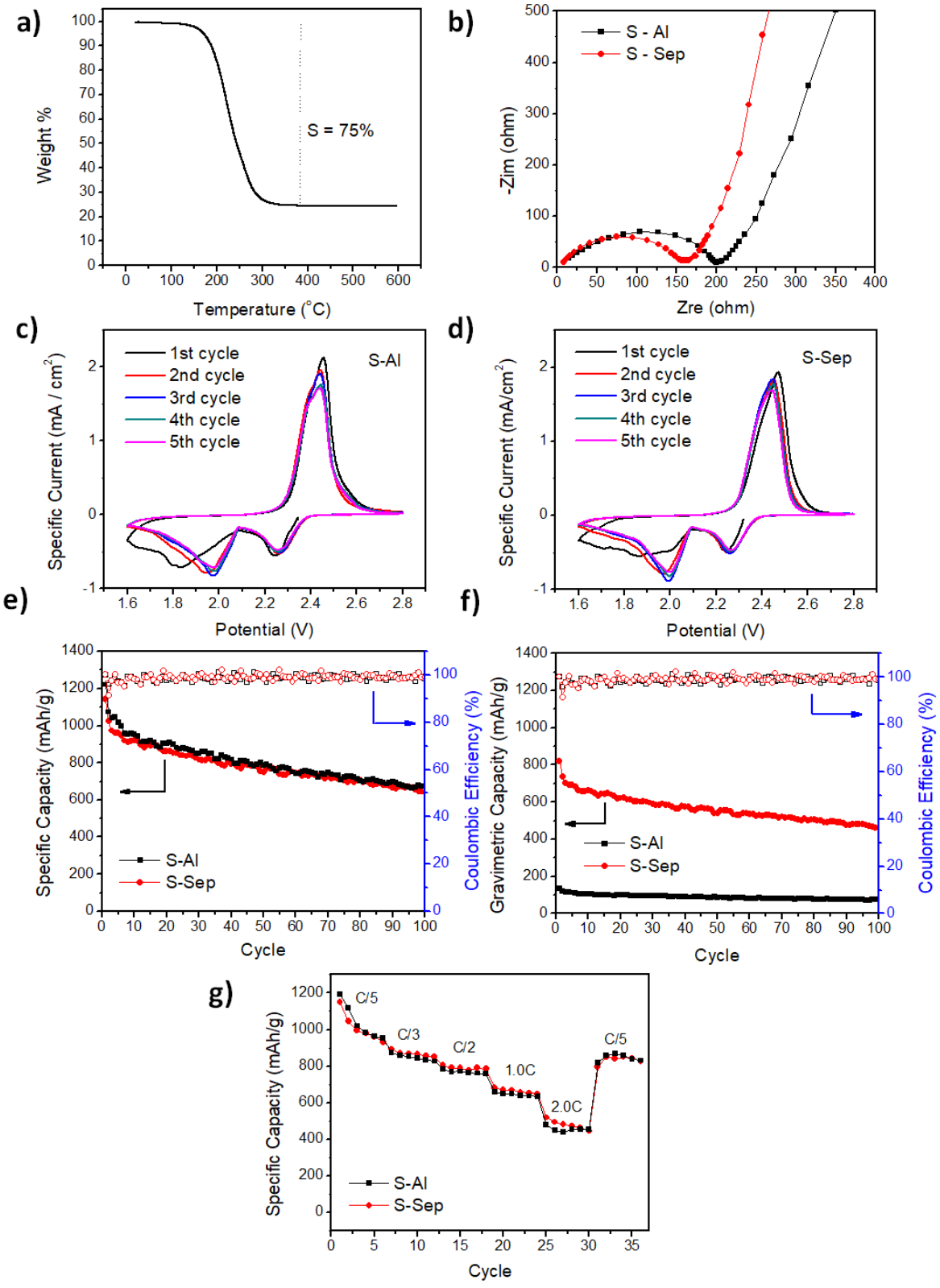
a)
Weight %
S = 75%
Temperature (°C)
b)
S - Al
S - Sep
-Zim (ohm)
Zre (ohm)
c)
1st cycle
2nd cycle
3rd cycle
4th cycle
5th cycle
S-Al
Specific Current (mA / cm²)
Potential (V)
d)
1st cycle
2nd cycle
3rd cycle
4th cycle
5th cycle
S-Sep
Specific Current (mA/cm²)
Potential (V)
e)
Specific Capacity (mAh/g)
Coulombic Efficiency (%)
S-Al
S-Sep
Cycle
f)
Gravimetric Capacity (mAh/g)
Coulombic Efficiency (%)
S-Al
S-Sep
Cycle
g)
C/5
C/3
C/2
1.0C
2.0C
C/5
Specific Capacity (mAh/g)
S-Al
S-Sep
Cycle

Fig. 4.4. **a)** TGA on sprayed sulfur. **b)** EIS characterization on S-Al and S-Sep. **c)** Cyclic voltammogram profiles on **c)** S-Al and **d)** S-Sep. **e)** Specific capacity and **f)** gravimetric capacity of S-Al and S-Sep calculated based on sulfur mass and total mass respectively. **g)** Rate capability of S-Al and S-Sep systems calculated based on sulfur mass.

After cycling was finished, the surfaces of both systems were analyzed with SEM (Figure 4.5a,b). The S-Al surface in Figure 4.5a was facing the separator, whereas the S-Sep surface in Figure 4.5b was facing the coin cell end cap, away from the lithium anode. S-Al shows a dense and packed morphology while S-Sep displays a porous structure. The change of S-Al structure from porous to dense might be attributed to the imaged surface was the first to be accessed by electrochemical reactions. The unchanged porous structure before and after cycling from S-Sep shows that no significant electrochemical reaction occurred furthest from the lithium anode. This may be due to the formation of dense electrode material layer on the separator side (similar to Figure 4.5a), restraining lithium ions from diffusing through the electrode, ultimately minimizing electrochemical reactions on the back side and preserving the porous structure.

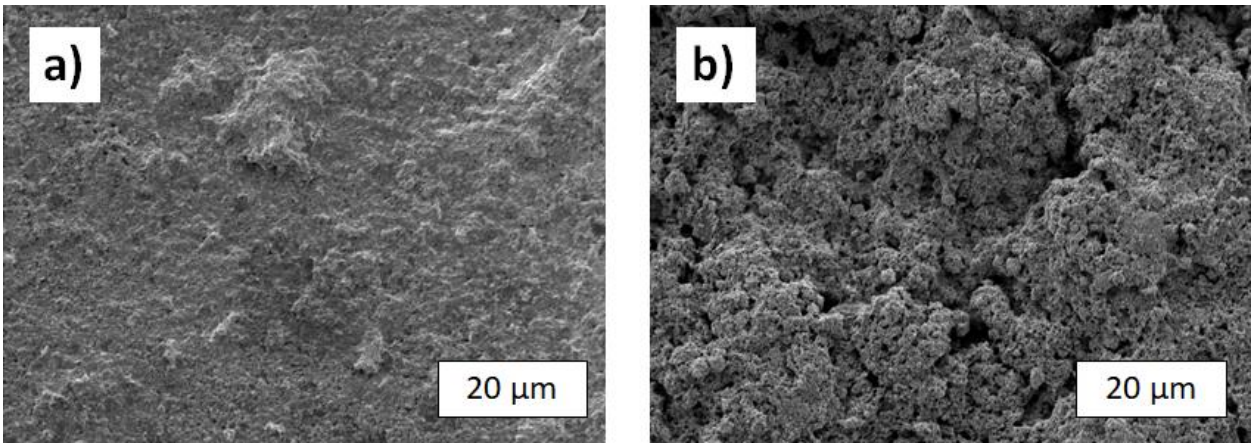

Fig. 4.5. Top view SEM images of **a)** S-Al and **b)** S-Sep.

4.4 Conclusion

Air-controlled electrospraying is a process which can be used to excellently coat various surfaces. By coating sulfur active material directly onto the separator, the need of an aluminum current collector in a Li-S battery was eliminated. By removing the current collector during assembly, gravimetric capacity was increased, offering potential to reduce production costs in future Li-S commercialization. In this work, we only employed a low sulfur loading for a proof of concept. To compete with conventional lithium-ion battery technology, higher sulfur loading with high capacity and excellent capacity retention is required. In future work, we will employ high sulfur loading with relatively high gravimetric energy density by depositing the active materials directly onto functional polymer materials, such as polyimide based separators. In addition, coating an extra carbon layer on the separator side facing the lithium anode offers potential to mitigate polysulfide diffusion even further

Acknowledgment

This work was funded by Axium Nano, LLC (Cornell OSP No. 80674) and Department of Energy (DOE EERE Battery500). All the material characterizations were obtained via facilities at the Cornell Center for Materials Research (part of NSF MRSEC Program, Grant DMR 1120296).

References

[1] M. Wild, L. O'Neill, T. Zhang, R. Purkayastha, G. Minton, M. Marinescu, G.J. Offer, Lithium-sulfur batteries, a mechanistic review, Energy Environ. Sci. 8 (2015) 3477–3494. doi:10.1039/C5EE01388G.

[2] R. Van Noorden, The rechargeable revolution: A better battery, Nature. 507 (2014) 26–28. doi:10.1038/507026a.

[3] A. Manthiram, Y. Fu, Y.-S. Su, Challenges and Prospects of Lithium–Sulfur Batteries, Acc. Chem. Res. 46 (2013) 1125–1134. doi:10.1021/ar300179v.

[4] D. Bresser, S. Passerini, B. Scrosati, Recent progress and remaining challenges in sulfur-based lithium secondary batteries--a review., Chem. Commun. (Camb). 49 (2013) 10545–62. doi:10.1039/c3cc46131a.

[5] X. Ji, K.T. Lee, L.F. Nazar, A highly ordered nanostructured carbon–sulphur cathode for lithium–sulphur batteries, Nat. Mater. 8 (2009) 500–506. doi:10.1038/nmat2460.

[6] A. Manthiram, Y. Fu, S.H. Chung, C. Zu, Y.S. Su, Rechargeable lithium-sulfur batteries, Chem. Rev. 114 (2014) 11751–11787. doi:10.1021/cr500062v.

[7] J. Wang, Y. Yang, F. Kang, Porous carbon nanofiber paper as an effective interlayer for high-performance lithium-sulfur batteries, Electrochim. Acta. 168 (2015) 271–276. doi:10.1016/j.electacta.2015.04.055.

[8] J. Zhu, Y. Ge, D. Kim, Y. Lu, C. Chen, M. Jiang, X. Zhang, A novel separator coated by carbon for achieving exceptional high performance lithium-sulfur batteries, Nano Energy. 20 (2016) 176–184. doi:10.1016/j.nanoen.2015.12.022.

[9] B.P. Williams, Y.L. Joo, Tunable Large Mesopores in Carbon Nanofiber Interlayers for High-Rate Lithium Sulfur Batteries, J. Electrochem. Soc. 163 (2016) A2745–A2756.

doi:10.1149/2.0931613jes.

[10] L. Ji, M. Rao, H. Zheng, L. Zhang, Y. Li, W. Duan, J. Guo, E.J. Cairns, Y. Zhang, Graphene oxide as a sulfur immobilizer in high performance lithium/sulfur cells, J. Am. Chem. Soc. 133 (2011) 18522–18525. doi:10.1021/ja206955k.

[11] X. Zhou, Y. Li, G. Ma, Q. Ma, Z. Lei, One-step solid-state synthesis of sulfur-reduced graphene oxide composite for lithium-sulfur batteries, J. Alloys Compd. 685 (2016) 216–221. doi:10.1016/j.jallcom.2016.05.171.

[12] M. Lao, G. Zhao, X. Li, Y. Chen, S.X. Dou, W. Sun, Homogeneous Sulfur–Cobalt Sulfide Nanocomposites as Lithium–Sulfur Battery Cathodes with Enhanced Reaction Kinetics, ACS Appl. Energy Mater. (2017) acsaem.7b00049. doi:10.1021/acsaem.7b00049.

[13] N. Mosavati, V.R. Chitturi, S.O. Salley, K.Y.S. Ng, Nanostructured titanium nitride as a novel cathode for high performance lithium/dissolved polysulfide batteries, J. Power Sources. 321 (2016) 87–93. doi:10.1016/j.jpowsour.2016.04.099.

[14] L. Fei, S.H. Yoo, R.A.R. Villamayor, B.P. Williams, S.Y. Gong, S. Park, K. Shin, Y.L. Joo, Graphene Oxide Involved Air-Controlled Electrospray for Uniform, Fast, Instantly Dry, and Binder-Free Electrode Fabrication, ACS Appl. Mater. Interfaces. 9 (2017) 9738–9746. doi:10.1021/acsami.7b00087.

[15] X. Li, J. Yang, Y. Hu, J. Wang, Y. Li, M. Cai, R. Li, X. Sun, Novel approach toward a binder-free and current collector-free anode configuration: highly flexible nanoporous carbon nanotube electrodes with strong mechanical strength harvesting improved lithium storage, J. Mater. Chem. 22 (2012) 18847. doi:10.1039/c2jm33297c.

[16] C. Mattevi, G. Eda, S. Agnoli, S. Miller, K.A. Mkhoyan, O. Celik, D. Mastrogiovanni, G. Granozzi, E. Carfunkel, M. Chhowalla, Evolution of electrical, chemical, and structural

properties of transparent and conducting chemically derived graphene thin films, Adv. Funct. Mater. 19 (2009) 2577–2583. doi:10.1002/adfm.200900166.

[17] J. Lee, B. Ko, J. Kang, Y. Chung, Y. Kim, W. Halim, J.H. Lee, Y.L. Joo, Facile and scalable fabrication of highly loaded sulfur cathodes and lithium–sulfur pouch cells via air-controlled electrospray, Mater. Today Energy. 6 (2017) 255–263. doi:10.1016/j.mtener.2017.11.003.

[18] N. Jayaprakash, J. Shen, S.S. Moganty, A. Corona, L.A. Archer, Porous hollow carbon@sulfur composites for high-power lithium-sulfur batteries, Angew. Chemie - Int. Ed. 50 (2011) 5904–5908. doi:10.1002/anie.201100637.

[19] L. Stobinski, B. Lesiak, A. Malolepszy, M. Mazurkiewicz, B. Mierzwa, J. Zemek, P. Jiricek, I. Bieloshapka, Graphene oxide and reduced graphene oxide studied by the XRD, TEM and electron spectroscopy methods, J. Electron Spectros. Relat. Phenomena. 195 (2014) 145–154. doi:10.1016/j.elspec.2014.07.003.

[20] C.T. Love, Thermomechanical analysis and durability of commercial micro-porous polymer Li-ion battery separators, J. Power Sources. 196 (2011) 2905–2912. doi:10.1016/j.jpowsour.2010.10.083.

[21] M. He, X. Zhang, K. Jiang, J. Wang, Y. Wang, Pure inorganic separator for lithium ion batteries, ACS Appl. Mater. Interfaces. 7 (2015) 738–742. doi:10.1021/am507145h.

[22] H. Yamin, A. Gorenshtein, J. Penciner, Y. Sternberg, E. Peled, Lithium Sulfur Battery: Oxidation/Reduction Mechanism of Polysulfides in THF Solutions, J. Electrochem. Soc. 135 (1988) 1045. doi:10.1149/1.2095868.

Chapter 5

Future Work

The idea of combining Lithium-sulfur cathodes and air-controlled electrospray in different applications has shown their potential and synergy based on the results presented. Due to time constraint, this project has not been fully explored and the scientific reasons behind some results haven't been explained or proved, especially for the Layer-on-Layer project. In the future work, effort is needed first to find an optimum structure and ratio of active material layer and graphene layer for better utilization of graphene materials with less hindrance for ion diffusion. Second, the layer effect can be investigated, like the influence to electrochemical performance with more layers at the same loading. Third, more layers can be stacked to fabricate cathodes with a sulfur loading of 5mg/cm^2 or more. Fourth, the idea of Chapter 3 and Chapter 4 can also be integrated to make current collector free cells with high loading and Layer-on-Layer structure.